Science of the Total Environment 706 (2020) 134864

Contents lists available at ScienceDirect

Science of the Total Environment

journal homepage: www.elsevier.com/locate/scitotenv

Ambient concentrations and total deposition of inorganic sulfur, inorganic nitrogen and base cations in the Athabasca Oil Sands Region

Eric S. Edgerton [a,*], Yu-Mei Hsu [b], Emily M. White [c], Mark E. Fenn [e], Matthew S. Landis [d]

[a] Atmospheric Research & Analysis, Inc., 410 Midenhall Way, Cary, NC, 27513, USA
[b] Wood Buffalo Environmental Association, 805 Memorial Drive, Fort McMurray, T9K0K4, Canada
[c] Maed Consulting, 151 Harrison Court, Pittsboro, NC, 27312, USA
[d] Integrated Atmospheric Solutions, LLC, 1009 Yellow Birch Drive, Cary, NC, 27519, USA
[e] USDA Forest Service, Pacific Southwest Research Station, 4955 Canyon Crest Drive, Riverside, CA, 92507, USA

HIGHLIGHTS

- Atmospheric concentration and deposition data from 2000 to 2017 were analyzed.
- Deposition of S, N and base cations was estimated for boreal jack pine sites.
- Highest ambient concentrations and deposition occurred near oil sand operations.
- Potential acid input exhibited a complex pattern dependent on local sources.
- Significant downward trends were observed for SO_2, less so for NO_2 and PM.

GRAPHICAL ABSTRACT

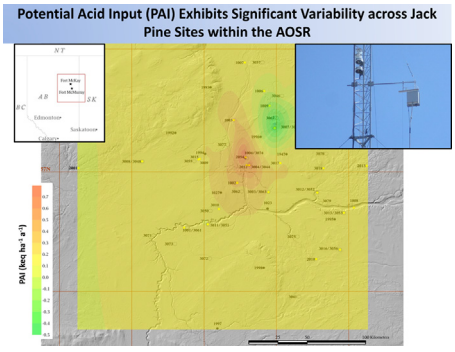

ARTICLE INFO

Article history:
Received 5 April 2019
Received in revised form 5 October 2019
Accepted 5 October 2019
Available online 18 November 2019

Guest Editor: Kelly Roland Munkittrick

Keywords:
Sulfur
Nitrogen
Base cations
Atmospheric deposition
Nitric acid
Ammonia
Boreal forest
Oil sands

ABSTRACT

Trace gas, particulate matter and deposition data collected in the Athabasca Oil Sands Region (AOSR) from 2000 to 2017 were evaluated as part of a broad scientific programmatic review. Results showed significant spatial patterns and temporal trends across the region. Concentrations of reactive gases were highest near the center of surface oil sands production operations and decreased towards the edges of the monitoring domain by factors of 8, 20, 4 and 3 for SO_2, NO_2, HNO_3 and NH_3, respectively. 18 of 30 sites showed statistically significant ($p < 0.05$) negative trends in SO_2 concentrations suggesting an ~40% decrease since 2000. In contrast, only 2 of 30 sites showed statistically significant temporal trends (1 positive, 1 negative) for NO_2. NH_3 data showed (i) intermittent wildfire impacts, and (ii) high seasonality, with low concentrations during winter and significantly higher values during the summer. PM_{10} measurements were more limited, but also showed significant spatio-temporal variability. Comparison of PM_{10} and $PM_{2.5}$ data showed that >80% of SO_4^{2-} was in the $PM_{2.5}$ fraction, while > 60% of Ca^{2+}, Mg^{2+}, Na^+ and Cl^- were in the $PM_{10-2.5}$ fraction. Ion balances of both PM_{10} and $PM_{2.5}$ contained cation excesses at near-field oil sand sites, but $PM_{2.5}$ samples at forest health sites >20 km from surface production locations contained anion excesses. Monthly average concentrations of PM_{10} ions showed peak Ca^{2+} during March-April to November, but peak SO_4^{2-}, NH_4^+ and NO_3^- from November-March. Deposition estimates showed rapid declines as a function of distance to oil sand operations. Estimated total N and total S deposition to forest health monitoring sites ranged from 2.0 to 5.7 kg ha^{-1} a^{-1} and 2.1–14.0 kg ha^{-1} a^{-1}, respectively. Potential acid input (PAI) ranged from −0.46 to 0.79 keq ha^{-1} a^{-1}

* Corresponding author.
E-mail addresses: eedgerton@atmospheric-research.com (E.S. Edgerton), mlandis@atmospheric-solutions.com (M.S. Landis).

https://doi.org/10.1016/j.scitotenv.2019.134864

and was mostly 0.1–0.2 keq ha^{-1} a^{-1} throughout the domain, except for two clusters of sites near oil sand operations.

1. Introduction

The Athabasca Oil Sands Region (AOSR) in northeastern Alberta, Canada contains the world's third largest proven oil reserve at 166 billion barrels. Approximately 20% of the reserve is considered mineable (i.e., within 70 m of the surface) and the other 80% requires in situ approaches (e.g., steam-assisted gravity drainage) for extraction. Commercial development of the oil sands began in the late 1960s with surface mining operations between Fort McKay and Fort McMurray (Foster et al., 2019). Total production from oil sands operations increased roughly 4-fold from 2000 to 2015 (6.1×10^5 barrels per day (bbl/day) to 2.4×10^6 bbl/day) and is projected to increase another 60% (3.9×10^6 bbl/day) by 2030 (Oil Sands Magazine, 2016).

Oil sand operations are the main source of air emissions in the AOSR. Heavy duty diesel shovels and trucks are major sources of NO_x (i.e., NO + NO_2), fine particulate matter and black carbon. Industrial operations for extracting and upgrading bitumen (raw oil sand) to crude oil are major sources of SO_2. Fugitive dust from mining operations, mine haul roads, quarries, highways and storage piles are significant sources of trace elements, base cations (BC), polycyclic aromatic hydrocarbons (PAHs) and polycyclic aromatic compounds (PACs) (Zhang et al., 2016; Landis et al., 2019). Fugitive dust emissions from these sources are poorly understood, both in terms of particle size distribution and total mass. NOx emissions in the AOSR were approximately 80 and 110 kilotons (kton), respectively, in 2000 and 2015 and are projected to increase to about 180 kton by 2030. In contrast, SO_2 emissions declined from 95 kton in 2000 to 70 kton in 2015 and are projected to increase to about 110 kton by 2030 (Foster et al., 2019).

Surrounding the oil sands operations are large areas of boreal forest growing on soils with low buffering capacity and lakes with low acid neutralizing capacity. In parallel with development, concern has grown about the effects of emissions from oil sands operations on potentially sensitive terrestrial and aquatic ecosystems. Substantial work has been done in the AOSR to understand sensitivity of soils, vegetation and lakes to these stressors (Foster et al., 2001; Percy et al., 2013; Macdonald, 2015), and to develop emission inventories (Zhang et al., 2018; Qui et al., 2018), deterministic models (Davies, 2012; Vijayaraghavan et al., 2016; Makar et al., 2018) and receptor models (Landis et al., 2012, 2017a, 2019) to estimate or predict deposition/exposure and to associate sources with sinks. Numerous studies and surveys has been conducted to document contaminant concentrations and trends in air (Hsu, 2013; Hsu et al., 2016; Davidson and Spink, 2018; Bari et al., 2016; Percy et al., 2012), snowpack (Murray, 1981; Guéguen et al., 2016), wet deposition (Barrie and Kovalick, 1980; Sandhu and Blower, 1986; Lynam et al., 2015), rivers and lakes (Kelly et al., 2010), lichens (Addison and Puckett, 1980; Landis et al., 2012, 2019), sphagnum moss (Shotyk et al., 2014, 2016) and other components of boreal ecosystems. In general, these studies have shown that emissions from the oil sands are detectable in various media (air, snowpack, lichen, moss) out to a distance of 20–50 km.

In the late 1990s, the Wood Buffalo Environmental Association (WBEA) initiated several programs for long-term monitoring of air quality, deposition and forest health in the AOSR (Foster et al., 2019). These were motivated by growing concerns about acidification and eutrophication or fertilization of surrounding ecosystems. The WBEA Terrestrial Environmental Effects Monitoring (TEEM) program established a region-wide passive sampling network in 1998–99 to monitor above-canopy concentrations of SO_2, NO_2, O_3, HNO_3 and NH_3 at Forest Health Monitoring (FHM) sites (Foster et al., 2019). TEEM deployed a second network in 2008 to measure bulk and throughfall deposition of inorganic acids and base cations at FHM sites, and a third network in 2013–17 to measure above canopy concentrations of gases and $PM_{2.5}$ composition at several solar-powered FHM sites. Taken together, these networks provide a relatively dense array of measurements for examining patterns and trends of deposition and air quality.

This paper presents and analyzes TEEM air and deposition data collected from 2000 through 2017, a period of rapid development in the oil sands. Observational data are used to examine temporal trends in gaseous and particulate sulfur (S), gaseous and particulate nitrogen (N) and BC across the AOSR using parametric and non-parametric statistics. TEEM data are also used to estimate total deposition of S, N and BC at TEEM FHM sites. Results are then compared with other monitoring networks in Canada, the U.S., UK and Europe. We also calculate potential acid input (PAI) for the TEEM FHM sites, referenced to the TEEM forest health survey conducted in 2011–12. PAI is a useful indicator of the relative deposition of total acids and total bases (i.e., net acidity or alkalinity) to forest ecosystems. PAI is also important from a regulatory perspective, because critical loads for PAI have been established for the Province of Alberta (Government of Alberta, 2012). Our approach for estimating PAI uses observational data at specific FHM sites, while the regulatory approach uses modelled data for discrete grid cells. Although these two approaches are not directly comparable, our findings are relevant because they shed light on deposition to one of the most sensitive receptors in the AOSR (i.e., jack pine stands).

2. Methods

Fig. 1 shows the region of interest and the sites that provided measurement data or served as receptors for deposition calculations. FHM sites have 4-digit identifiers and community or industrial sites have 4-letter identifiers. Information and associated measurements for TEEM FHM sites are listed in Appendix Tables A.1 and A.2.

2.1. Ambient air concentrations

2.1.1. Passive measurements of gaseous SO_2, NO_2, HNO_3 and NH_3

Passive samplers were used to measure sulfur dioxide (SO_2), nitrogen dioxide (NO_2), nitric acid (HNO_3) and ammonia (NH_3) at community, industrial and FHM sites (see Appendix Table A.1). SO_2 and NO_2 were measured with samplers developed by Tang et al. (1997 and 1999); HNO_3 and NH_3 were measured with Ogawa (Pompano Beach, FL) style samplers (Hsu, 2013).

The passive sampling network included 11–13 sites from 2000 to 2007, 23–28 sites from 2008 to 2012, and 30–35 sites from 2013 to 2017 (see Foster et al., 2019 for rationale and details). At FHM sites, samplers were exposed on towers several meters (m) above the forest canopy (roughly 25 m above ground level, agl). At non-FHM sites, samplers were exposed in forest clearings, roughly 5 m agl. Duplicate samples were collected at roughly half of the

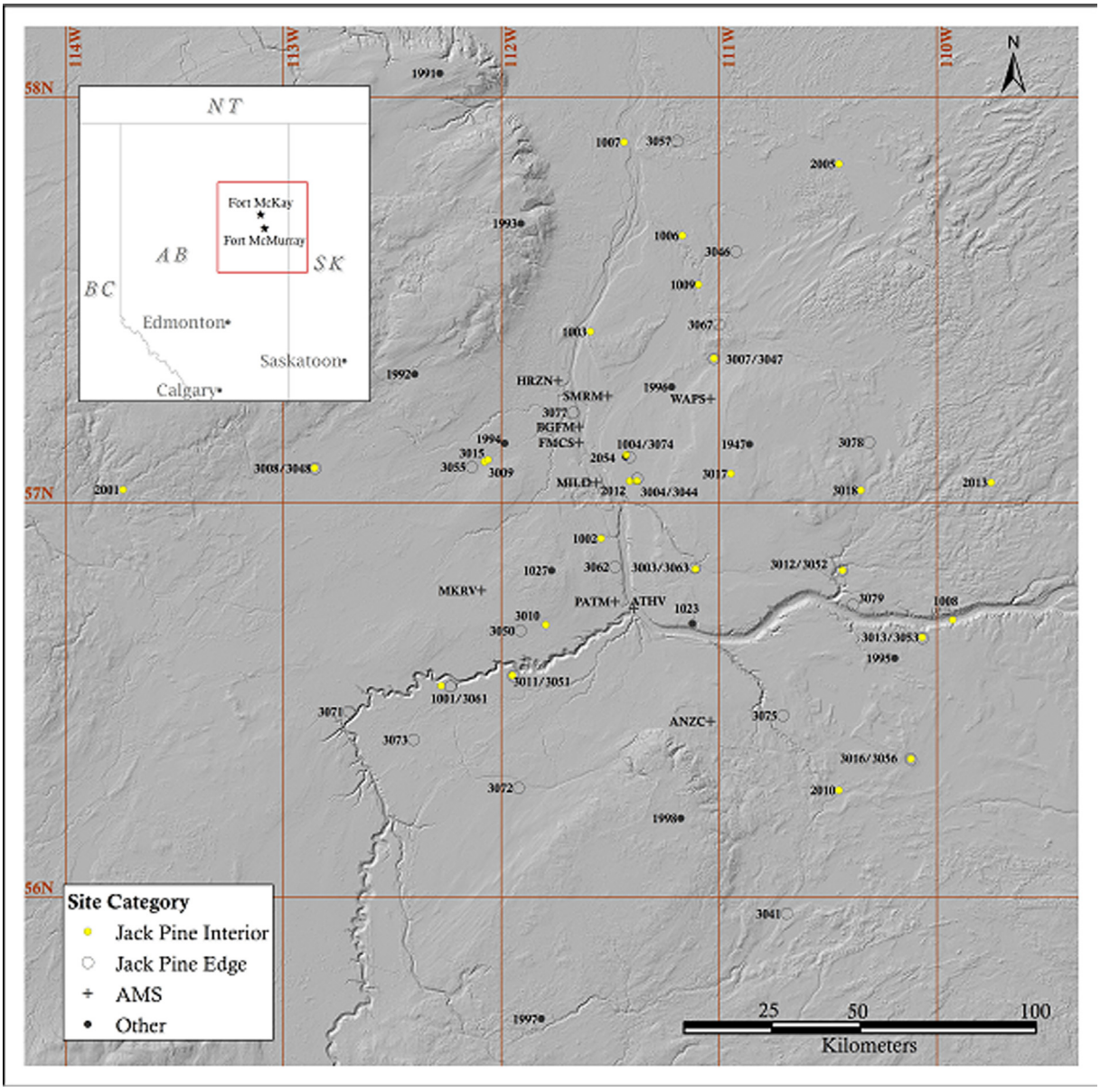

Fig. 1. Locations of monitoring and receptor sites used in this study. TEEM FHM sites have 4-digit ID, community and industrial sites have 4-letter ID.

sites, and multiple travel blanks were collected with each sample batch. Exposure times were approximately 1-month during the warm season (April–September) and 2-months during the cold season (October–March).

Samples and blanks were extracted in >18.2 MΩ cm deionized water and analyzed for sulfate (SO_4^{2-}), nitrite (NO_2^-), nitrate (NO_3^-) and ammonium (NH_4^+) using a Dionex (Sunnyvale, CA) Model 300 ion chromatograph (IC). Loadings of SO_4^{2-}, NO_2^-, NO_3^- and NH_4^+ were converted to SO_2, NO_2, HNO_3 and NH_3, respectively, based on exposure time and an empirically derived effective flow rate that was a function of ambient temperature, wind speed and relative humidity (Hsu, 2013). Detection limits (LDs) were 0.1 ppb for SO_2, NO_2, NH_3, and 0.02 ppb for HNO_3.

2.1.2. Filter-based measurements of $PM_{2.5}$ and PM_{10}

PM (particulate matter) samples for chemical analysis were collected at four community sites and three industrial sites operated by WBEA from 2009 to 2017. The community sites sampled $PM_{2.5}$ and PM_{10}, while the industrial sites sampled only PM_{10}. Sampling followed the Environment Canada National Air Pollution Surveillance (NAPS) 1-in-6-day, 24-hour schedule (Environment Canada, 2012). Samples were collected on pre-weighed 47 mm diameter ringed Teflon filters (Whatman prior to 2015; MTL from 2015 forward) using ThermoScientific Partisol 2000 U.S. EPA Federal reference method air samplers. Lab blanks and travel blanks were prepared and analyzed with each batch.

Following exposure, filters were returned to the laboratory, equilibrated in a humidity- and temperature-controlled Class 1000 clean room and re-weighed to determine net loadings of $PM_{2.5}$ and PM_{10} mass. Samples and blanks were then extracted in 30 mL of >18.2 MΩ·cm deionized water and analyzed for anions: fluoride (F^-), chloride (Cl^-), NO_3^-, ortho-phosphate (PO_4^{3-}), SO_4^{2-} and cations: NH_4^+, sodium (Na^+), potassium (K^+), calcium (Ca^{2+}) magnesium (Mg^{2+}) with a Dionex Model ICS-3000 IC, as described in Landis et al. (2017a).

LDs ranged from 0.001 μg m^{-3} for NH_4^+ and Mg^{2+} to 0.010 μg m^{-3} for SO_4^{2-} and Ca^{2+}. NO_3^- concentrations from these measurements should be considered lower limit estimates, due to potential loss

of volatile nitrates from Teflon filters (Seinfeld and Pandis, 1998; Landis et al., 2001; Edgerton et al., 2006).

2.1.3. Denuder/filter pack measurements for HNO_3, NH_3 and fine particulate sulfate (pSO_4^{2-}), nitrate (pNO_3^-) and ammonium (pNH_4^+)

Annular denuder systems (ADS) for above-canopy (i.e., 25 m agl) measurements of HNO_3 and NH_3 were installed at four solar-powered FHM sites (1 central, 3 remote) in mid-2013. The central site (site 1004) was ~20 km east of major point and area sources and the three remote sites were 100–125 km north (site 1007), west (site 2001) and east (site 2013) of site 1004 (see Fig. 1).

The ADS consisted of two URG Corporation (Chapel Hill, NC) 150 mm long by 30 mm diameter annular denuders in series (KCl for HNO_3 and citric acid for NH_3) followed by a mass flow meter, a low-power pump and a thermostatically-controlled heater to keep the pump from seizing at low temperatures. Sample flow was 1.0–1.2 l min^{-1}, and the system consumed <10 W and <20 W with the heater off and on, respectively. Samplers ran continuously for nominal 1 or 2 month collection periods (Aug–Nov 2013; Jun–Dec 2014; year-round from 2015 to 2017).

In January 2017, an in-line cyclone with a 2.5 μm cut-point and a 2-stage filter pack were added downstream of the denuders for measurement of pSO_4^{2-}, pNO_3^- and pNH_4^+. The filter pack had a Teflon pre-filter to collect non-volatile PM and a nylon backup filter to capture volatile nitrate (U.S. EPA, 1999).

Denuders and filters were extracted in 10 mL and 30 mL, respectively, of > 18 MΩ-cm deionized water, then analyzed for SO_4^{2-}, NO_3^- and NH_4^+ with a Dionex Model ICS-3000 IC following USEPA Method IO-5.0 (USEPA, 1999). LDs for monthly samples (nominal 50 m^3 volume) were < 0.01 ppb for HNO_3, 0.03 ppb for NH_3, <0.01 μg m^{-3} for pSO_4^{2-} and pNH_4^+ and 0.02 μg m^{-3} for pNO_3^- (sum of Teflon and nylon filters).

2.2. Deposition measurements and estimates

2.2.1. Ion exchange resins for bulk deposition and throughfall

Ion exchange resin collectors (IERs) were used to measure bulk deposition and throughfall deposition of inorganic sulfur and nitrogen (SO_4^{2-}, NO_3^-, NH_4^+) and base cations (BC = Ca^{2+}, K^+, Mg^{2+} and Na^+) as described by Fenn et al. (2015). Measurements of sulfur and nitrogen (S/N) deposition began in late 2008 and continued to the present. Measurements of BC covered two time periods: late 2008 through early 2010, and late 2013 to the present. Table A.2 lists the sites and associated periods of record for S/N and BC measurements.

Bulk samplers (3–5 per site) were installed in clearings adjacent to FHM sites and throughfall collectors (3–8 per site) were installed under the jack pine canopy within FHM sites. Field blanks were collected with each sample batch and used to blank-correct bulk and throughfall deposition. Sampling and analytical approaches for the TEEM program are described in detail by Fenn et al. (2015, 2018). LDs, based on 2 times the standard deviation of field blanks, were ≤0.03 kg per hectare (kg ha^{-1}) for NH_4^+-N and NO_3^--N, 0.08 kg ha^{-1} for SO_4^{2-}-S and ≤ 0.04 kg ha^{-1} for Ca^{2+}, Mg^{2+}, K^+ and Na^+.

2.2.2. Dry deposition calculations

Dry deposition fluxes of nitrogen species (NO_2, HNO_3, NH_3, pNH_4^+ and pNO_3^-) were calculated using the Multi-Layer Dry Deposition Model (MLM) developed by the U.S. National Oceanic and Atmospheric Administration (Meyers et al., 1998). Implementation of MLM and calculation of fluxes for calendar years 2015–2017 was performed as described by Hsu et al. (2016). Hourly meteorological variables (wbea.org) for the MLM were collected at the FHM and AMS sites. This version of the MLM did not incorporate bi-directional flux for NH_3, because the parameters used to estimate compensation points were not measured in the TEEM program. A recent modelling exercise (Whaley et al., 2018) investigated deposition across the AOSR with and without application of bi-directional fluxes for NH_3. Results showed the bi-directional flux approach decreased NH_3 deposition in some locations, but did not increase NH_3 deposition anywhere in the model domain.

2.2.3. Calculation of S, N, BC and PAI deposition

Working definitions for S, N, BC and PAI deposition are shown in Equations 1–4. Throughfall SO_4^{2-}-S measurements were used directly to estimate total sulfur deposition (Sdep). The sum of bulk NO_3^--N and bulk NH_4^+-N, plus modeled dry deposition of NO_2, HNO_3, NH_3, pNH_4^+ and pNO_3^- was used to estimate total nitrogen deposition (Ndep). Throughfall Ca^{2+} and Na^+ were used directly to estimate BC deposition (BCdep), while throughfall K^+ and Mg^{2+} were adjusted downward (adjK^+ and adjMg^{2+}) to account for canopy additions (see SI and Appendix Figure A.1), then included in the calculation of BCdep. For bulk N deposition and throughfall S deposition average annual values for the period 2009–2012 were used. For throughfall BC deposition, we used average annual values for the bracketing years 2009 and 2014. For modelled dry deposition of NO_2, HNO_3 and NH_3, we used the average of 2015 and 2016, and for modelled dry deposition of pNH_4^+ and pNO_3^- we used 2017 only, since this was the only year with regional PM measurements from the ADS.

$$\mathrm{Sdep} = \mathrm{Sdep_W} + \mathrm{Sdep_D} \sim \mathrm{Sdep_B} + \mathrm{Sdep_D} \sim \mathrm{Sdep_{TF}} \quad (1)$$

where,

$\mathrm{Sdep_W}$ = measured or modelled wet S deposition, kg − S $ha^{-1}a^{-1}$
$\mathrm{Sdep_D}$ = measured or modelled dry S deposition, kg − S $ha^{-1}a^{-1}$
$\mathrm{Sdep_B}$ = measured bulk S deposition, kg − S $ha^{-1}a^{-1}$
$\mathrm{Sdep_{TF}}$ = measured throughfall SO_4^{2-} − S deposition, kg − S $ha^{-1}a^{-1}$

$$\mathrm{Ndep} = \mathrm{Ndep_W} + \mathrm{Ndep_D} \sim \mathrm{Ndep_B} + \mathrm{Ndep_D} \quad (2)$$

where,

$\mathrm{Ndep_W}$ = measured or modelled wet N deposition, kg-N ha^{-1} a^{-1}
$\mathrm{Ndep_D}$ = measured or modelled dry N deposition, kg-N ha^{-1} a^{-1}
$\mathrm{Ndep_B}$ = measured bulk NO_3^- + bulk NH_4^+ deposition, kg-N ha^{-1} a^{-1}

An alternative approach for estimating Ndep that has been used by several researchers is to scale bulk nitrogen deposition based on the ratio of conservative ions, such as SO_4^{2-} or Na^+, in throughfall and bulk deposition (Fenn et al., 2013; Ferm and Hultberg, 1999). This approach is useful when measurements of nitrogenous gases and particles are unavailable; however, it assumes that total dry deposition of nitrogen species has the same spatial scale as that for SO_4^{2-} or Na^+. Test calculations using SO_4^{2-} as the conservative tracer showed similar results to Eq. (2), but with ~10–20% higher total N deposition at sites close to oil sand operations.

$$\mathrm{BCdep} = \mathrm{BCdep_W} + \mathrm{BCdep_D} \sim \mathrm{BCdep_B} + \mathrm{BCdep_D} \sim \mathrm{BCdep_{TF}} \quad (3)$$

where the components of BC are the four cations: Na^+, Ca^{2+}, adjK^+ and adjMg^{2+}units are kilo-equivalents ha^{-1} a^{-1} (keq ha^{-1} a^{-1})

PAI was then calculated using Eq. (4) as the sum of acidifying components minus neutralizing components.

$$\mathrm{PAI} = \mathrm{Sdep} + \mathrm{Ndep} - \mathrm{BCdep} \quad (4)$$

where all are expressed as keq ha^{-1} a^{-1}

This PAI calculation differs in several ways from that required by the Alberta acid deposition management framework for regulatory assessment (Government of Alberta, 2008, 2014). First, the

Alberta approach specifies a regional atmospheric deposition model to estimate Sdep, Ndep and BCdep, and we used observational data for these estimates. Second, the Alberta approach calculates PAI for a model domain of 1° by 1° grid cells covering Alberta and portions of neighboring provinces and states, while this study calculates point estimates for specific jack pine sites. Finally, the Government of Alberta uses PAI as a tool for management of acidifying emissions. The objective of the current work is to show patterns and trends across the AOSR and to provide input data for researchers studying associations between deposition and soil chemistry, foliar chemistry and plant communities (e.g., Bartels et al., 2019, this issue).

2.3. Statistical analyses

Data processing and statistical analyses were performed using SAS v.9.4 (SAS Institute, Cary, NC) and SigmaPlot v13 (Systat Software Inc., San Jose, CA). Parametric statistics used in this analysis include least square general linear model regression, a t-test for independent samples, and one-way analysis of variance (ANOVA). The assumptions of the parametric procedures were examined using residual plots, skewness and kurtosis coefficients, Shapiro-Wilk test, and Q-Q plots. Non-parametric statistics included Kendall tau for statistical significance and Sen's slope for changes over time. One-sided tests and a level of significance of $\alpha = 0.05$ were used for all statistical procedures unless otherwise stated. Spatial interpolation plots were created in Surfer v.15 (Golden Software, Golden, CO). Data were log transformed prior kriging, and displayed as linear in the subsequent figures. All data were blank-corrected based on loadings reported for field blanks. Time-weighted annual averages were calculated for passive trace gas data and ADS data to account for variable exposure periods.

3. Results and discussion

3.1. Spatial patterns of SO_2, NO_2, HNO_3 and NH_3

Summary statistics for SO_2, NO_2, HNO_3 and NH_3 are shown in Appendix Tables A.3–A.6. For SO_2, long-term time-weighted average concentrations ranged from 0.30 ppb at a remote site (site 1008) to 2.76 ppb at a centrally located industrial site (MILD). Nine of 36 sites (25%) reported average concentrations <0.5 ppb and 12 sites (33%) reported average concentrations > 1.0 ppb. Long-term average NO_2 concentrations ranged from 0.17 ppb at site 1991 to 5.78 ppb at MILD. Thirteen sites (36%) reported concentrations <0.5 ppb and 16 sites (44%) reported concentrations >1.0 ppb.

Multi-year (2014–2017) average NH_3 concentrations ranged from 0.19 ppb at site 2001 to 1.1 ppb at MILD. 18 of 36 sites (50%) exhibited long-term concentrations < 0.3 ppb, while 7 of 36 sites (19%) exhibited concentrations greater than 0.5 ppb. HNO_3 exhibited a relatively narrow factor of 2 range in concentrations across the network (0.07 ppb at site 1995 and 0.15 ppb at site 1004). Minimum and maximum concentrations were < 0.08 ppb for 7 sites 0.12–0.15 ppb for 8 sites (22%), respectively.

Annual 2017 time-weighted average concentrations of SO_2, NO_2, HNO_3 and NH_3 are shown in Appendix Figure A.2. All gases exhibit maximum concentrations near the center of oil sand operations and minimum concentrations at remote sites to the northwest and west. Data for SO_2 and NO_2 show a distinct southwest to northeast alignment of concentrations above 1.0 ppb. This pattern reflects mining development north of Fort McKay, but also mirrors the orientation of the Athabasca River valley. Wind direction in the valley has a strong preference for southwest and northeast and thus appears to contribute to higher concentrations in both these directions.

3.2. Temporal trends in SO_2, NO_2, HNO_3 and NH_3

Regression statistics for annual time-weighted average SO_2 versus year are summarized in Appendix Table A.7. Non-parametric and parametric tests for trends generally yield similar slopes, but with slightly lower p values (i.e., greater number of significant results) for the parametric tests. The 18-year group show statistically significant temporal trends for 5 of 6 sites, with downward slopes all on the order of −2.5% per year (roughly −0.06 ppb per year). Regression slopes imply an overall reduction in SO_2 concentrations of about 35–50% over the 18-year period of record. Results are consistent with findings from Feng at al. (2019) and Tang et al. (2018) who analyzed SO_2 trends in eastern Canada/U.S. and the UK, respectively. Feng at al. (2019) reported overall SO2 reductions of 88% between 1990 and 2015, while Tang et al. (2018) reported reductions of 81%. Aas et al. (2019) analyzed global and regional SO_2 observations for the period 2000–2015 and reported similar downward trends for North America (−4.7% per year) and Europe (−3.9% per year), no trend for east Asia (0.1% per year) and an upward trend for Africa (5.0% per year).

The 10–12-year group shows statistically significant decreases in SO_2 for 8 of 15 sites, plus borderline significance ($p < 0.1$) for another 2 sites, with regression slopes from −2.0 to −11.4% per year. The 4–8-year group shows statistically significant decreasing trends for 2 out of 4 sites, with slopes ranging from −4.3% per year to −12.1% per year. Unlike the FHM sites, none of the five WBEA community/industrial sites shows a statistically significant trend for SO_2.

Example time series of annual time-weighted SO_2 concentrations for 4 sites (3 significant trends, 1 non-significant trend) from the 18-year group are presented in Appendix Figure A.3. Concentrations in 2012 generally stand out as lower than 2013 and most years between 2014 and 2017. This is noteworthy because emission inventories indicate a ~40% decrease in SO_2 emissions within the AOSR between 2012 and 2013 and stabilization at still lower levels between 2014 and 2016 (Foster et al., 2019).

Regression statistics for annual average NO_2 versus year show few temporal trends (see Appendix Table A.8). Within the 18-year group, 2 of 6 sites show significant trends, but with slopes of opposite sign. No significant trend is observed for sites with <18 years of data. Like SO_2, a large proportion of regression slopes are negative. This suggests widespread decreases in NO_2 concentrations, but insufficient statistical power at individual sites to achieve significance. Time series plots of annual NO_2 concentrations for 4 example sites (2 significant upward trends, 1 significant downward trend and 1 non-significant trend) from the 18-year group are presented in Appendix Figure A.4.

The absence of NO_2 trends contrasts with AOSR emission inventories, which show ~25% increases in NO_2 emissions from 2005 to 2010 and again from 2010 to 2015 (Foster et al., 2019). However, province-wide NO_2 emissions decreased from 2000 through 2015 (Foster et al., 2019). Results for the passive NO_2 network also differ from Canada-wide trends. Reid and Aherne (2016) recently analyzed data from 63 regulatory monitoring sites across Canada with at least 10 years of data. Results showed significant (~35%) overall decreases between the years 1998 and 2013, more or less in accordance with national transportation emissions reductions.

Three-year average concentration fields of SO_2 and NO_2, for six time periods between 2000 and 2017 (2000–2002, etc.) are shown in Fig. 2 and Fig. 3, respectively. The passive network expanded significantly from 2000 to 2017, so the figures reflect the increased number of sites, expansion of the domain, and temporal variability. During the first two triennial periods, there were two sites with average SO_2 > 2 ppb and concentrations were mostly >1 ppb. The next two triennial periods show decreased concentrations and, by 2009–11, disappearance of the 2 ppb isopleth.

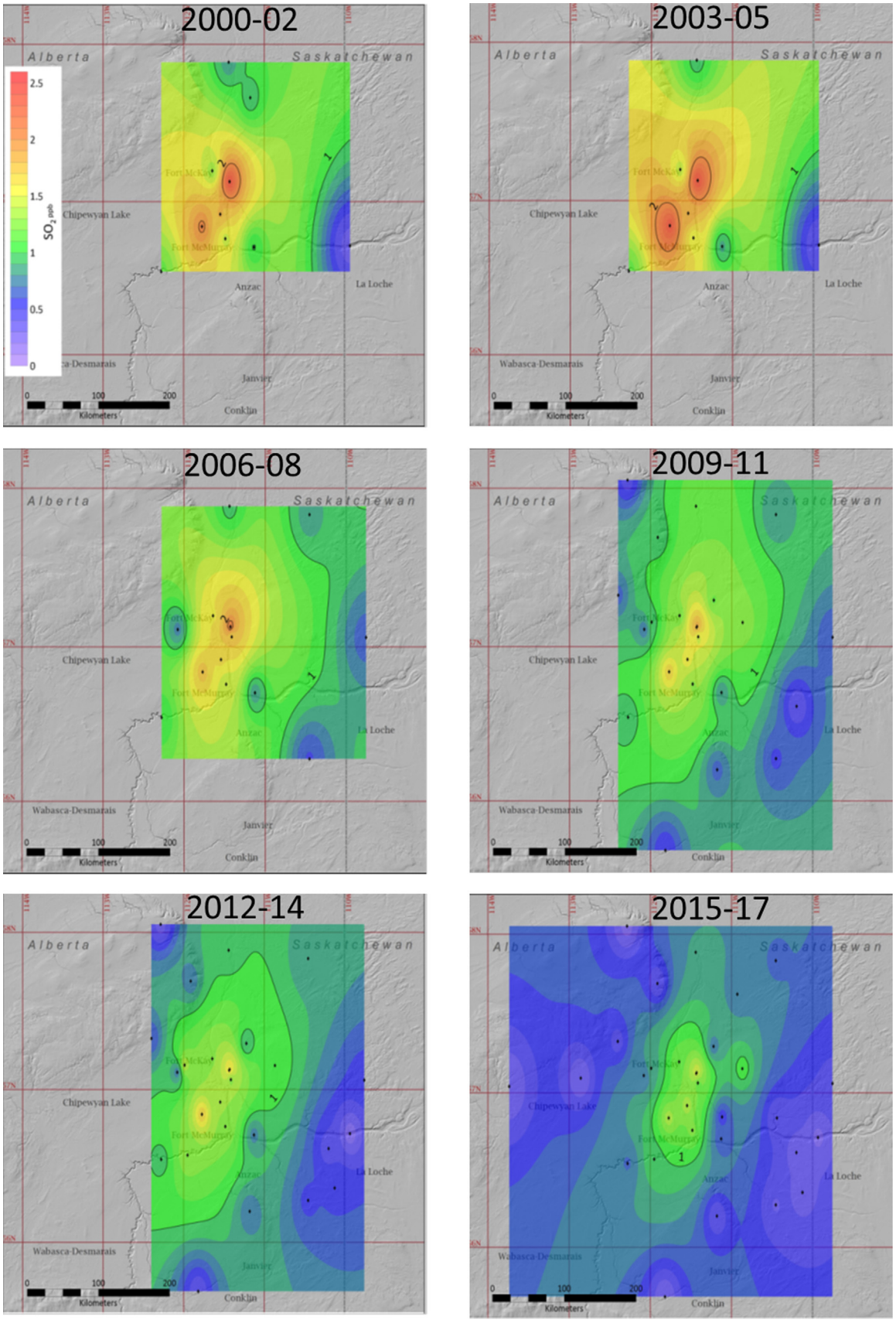

Fig. 2. Spatially Interpolated 3-year average SO_2 concentrations (ppb) from passive monitoring sites.

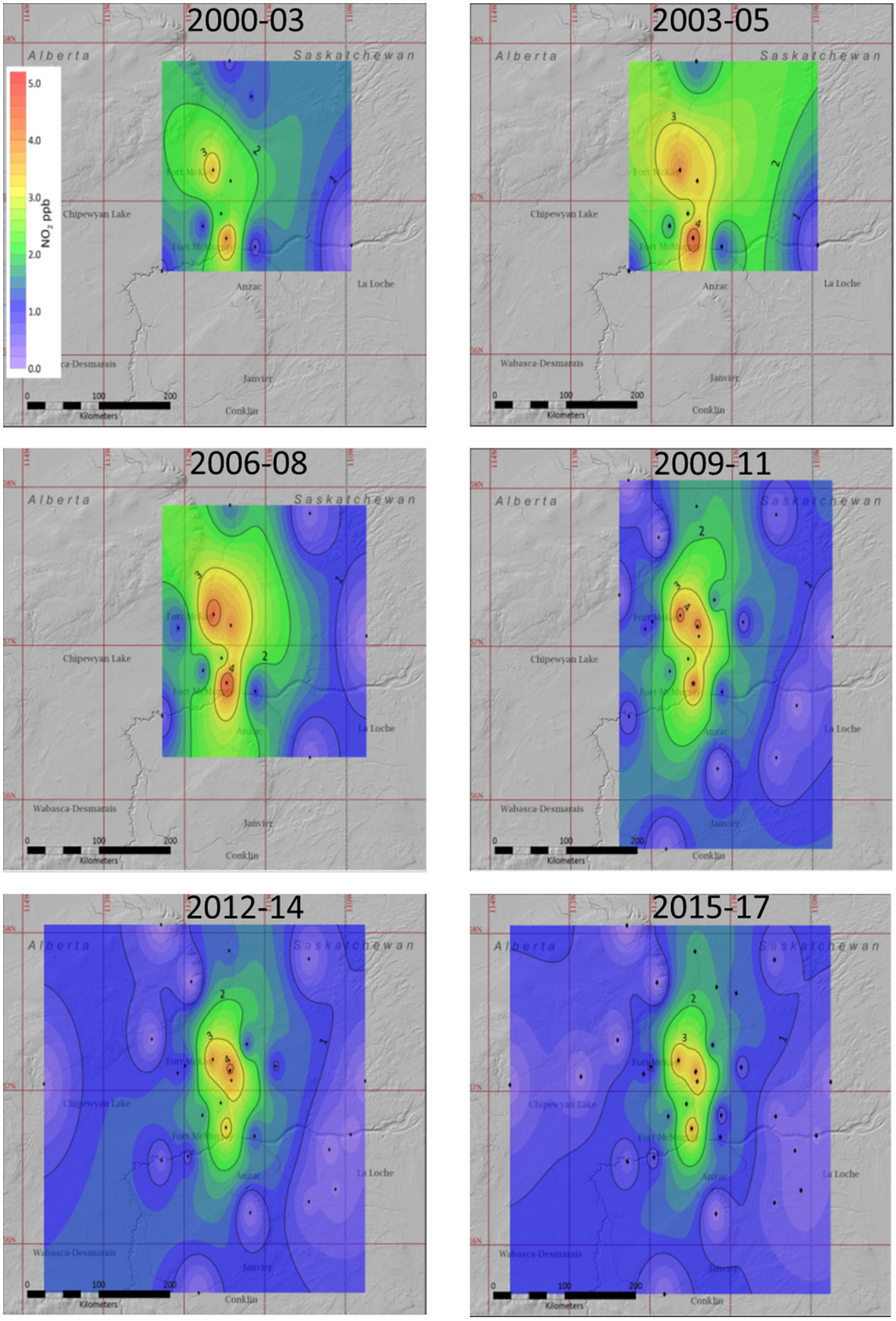

Fig. 3. Spatially Interpolated 3-year average NO_2 concentrations (ppb) from passive monitoring sites.

The last two triennial periods show a continued decline with concentrations >1 ppb confined to 6 sites near the center of the domain, plus 1 site located to the northeast.

NO_2 concentrations showed an increase at many sites for the first three time periods then a decline for the last three. The 2015–17 concentration field is similar to the 2000–03 field, but with improved definition of isopleths due to increased spatial coverage and site density.

The measurement record for HNO_3 and NH_3 was too short to test for annual trends; however, the data did indicate month to month and season to season variability. Monthly average concentrations of HNO_3 and NH_3 for the four sites with ADS are presented in Appendix Figure A.5. HNO_3 data show fairly well defined seasonal differences and differences between sites from late 2013 through 2015. During this time maxima (>0.15 ppb) occurred mid-year (summer) and minima (<0.05 ppb) occurred in winter. The typical order of concentration across sites was central ≥ north > east > west. Starting in late 2015, the month to month pattern became much less clear and maxima occurred at various times of the year. HNO_3 concentrations at the central and northern still exhibited the highest concentrations in most months, but more often than not north > central.

Monthly NH_3 concentrations showed more dramatic seasonality. The general pattern was one of low concentrations (<0.1 ppb) throughout the winter, an increase in early spring or about the time of smowmelt, high concentrations (≥0.25 ppb) during the summer, then a gradual decrease through the fall. Excursions with concentrations ≥ 1 ppb also occurred in different months in different years. These excursions usually involved multiple sites, but rarely all four sites. In 2016, for example, the Horse River Wildfire burned from early May through June and the single sample covering this period more than doubled the annual average concentrations at the central, northern and eastern sites. The western site (2001) showed little or no influence from the fire and evidently was upwind during much of the period. Box plots of annual average NH_3 concentrations from the passive samplers show that about half of the network was significantly affected by the Horse River Fire (see Appendix Figure A.6).

Low wintertime concentrations of NH_3 might be the result of reduced emissions from snow covered, frozen ground and limited biological activity. In addition, cold temperatures promote the formation of particulate NH_4NO_3 from HNO_3 and NH_3 (Seinfeld and Pandis, 1998) which can essentially titrate the less abundant precursor gas to near-zero concentration. A similar seasonal pattern was observed by Li et al. (2014) for a site in rural Wyoming, USA and they too attributed low wintertime NH_3 concentrations to particulate formation.

3.3. Comparison with literature values of NH_3, NO_2, HNO_3 and SO_2

TEEM NH_3, NO_2, HNO_3 and SO_2 measurements are compared with literature values in Table 1. Literature and publicly available data were included in the comparison if the data record included ≥1 year of measurements, sites were located in the Northern Hemisphere and settings were described as rural, regional or remote. Data from urban sites (high NO_x and photochemical products), agricultural sites (high NH_3) and livestock feedlots or poultry operations (high NH_3) were intentionally excluded because concentrations in these settings are known to be many times higher than those in the AOSR. The data in Table 1 are not meant to be an exhaustive compilation, but rather a basis for comparing TEEM results with those from potentially similar rural sites in the Northern Hemisphere.

The Environment and Climate Change Canada Canadian Acid Precipitation Monitoring Network (CAPMoN) measures particles and gases on a daily schedule using a three-stage open-faced filter pack (particle size cut unspecified) operated at 17 L per minute (lpm). Particles are collected on a Teflon filter, HNO_3 and a portion of SO_2 are collected on a nylon backup filter and the remaining SO_2 is collected on carbonate-impregnated final filters (Cheng and Zhang, 2017). The USEPA Clean Air Status and Trends Network (CASTNet) measures particles and gases on a weekly schedule

Table 1
Comparison of TEEM NH_3, NO_2, HNO_3 and SO_2 with literature values.

Location (Program)	Meas. Period	Method	Setting	Concentration ($\mu g\ m^{-3}$)				Ref.
				NH_3	NO_2	HNO_3	SO_2	
AOSR, CA (WBEA-TEEM)	2017	P	remote (n = 6)	0.10	0.87	0.21	0.97	this study
	"		central (n = 3)	0.16	7.73	0.31	3.78	"
AOSR, CA (WBEA-TEEM)	2017	D	remote (n = 3)	0.08	n.m.	0.18	n.m.	"
	"		central (n = 1)	0.17	n.m.	0.26	n.m.	"
Saturna, BC, CA (ECCC-CAPMoN)	2010	FP	regional	n.m.	n.m.	0.53	1.62	CAPMoN, 2019
Bratt's Lake, SK, CA (ECCC-CAPMoN)	"	"	regional	n.m.	n.m.	0.56	1.46	"
ON, CA (ECCC-CAPMoN)	"	FP	regional (n = 7)	n.m.	n.m.	0.06–0.81	0.14–2.41	"
So. Ontario, CA	2010–11	P	background (n = 1)	0.17	2.8	0.33	n.m.	Zbieranowski and Aherne, 2012
E. USA (USEPA-CASTNet)	2017	FP	regional (n = 54)	n.m.	n.m.	0.30–0.85	0.29–1.45	CASTNet, 2019
W. USA (USEPA-CASTNet)	2017	"	regional (n = 32)	n.m.	n.m.	0.16–1.21	0.17–0.78	"
USA (NADP-AMoN)	2015–17	P	rural (lowest 10%)	0.14–0.26	n.m.	n.m.	n.m.	NADP, 2019
"			other (top 90%)	0.76–15.	n.m.	n.m.	n.m.	"
Europe (EU-Nitro Europe IP)	2007–08	D	forest (n = 29)	0.12–4.75	0.69–30.	0.18–1.84	n.m.	Flechard et al., 2011
UK (UK-AGANET)	2015	D	rural bgnd (n = 28)	0.06–5.9	n.m.	0.05–0.53	0.10–0.59	UK-AGANET, 2019
W. USA	2011–12	FP	remote	0.15	n.m.	n.m.	n.m.	Chen et al., 2014
Alabama, USA	2016	C	rural-forested	0.23	2.5	0.46	0.89	SEARCH, 2019
Rocky Mtn. NP, USA	2008–09	D	alpine	0.23	n.m.	0.24	n.m.	Thompson et al., 2015
Wyoming, USA	2003–11	D	rural	0.17	n.m.	0.19	n.m.	Li et al., 2014
N. Sweden	2003–08	FP	rural northern	0.05	n.m.	0.12	0.12	Ferm and Hellsten, 2012
Tibet	2006–14	D	background	0.36	1.3	0.44	n.m.	Xu et al., 2015

P = passive; D = denuder; FP = filter pack; C = continuous; n.m. = not measured
ECCC-CAPMoN = Environment and Climate Change Canada Canadian Acid Precipitation Monitoring Network;
USEPA-CASTNet = U.S. Environmental Protection Agency Clean Air Status and Trends Network; NADP-AMoN = National Acid Deposition Program Ammonia Monitoring Network
EU-Nitro Europe IP = European Union Nitro Europe Integration Program; UK-AGANET = UK Acid Gases and Aerosol Network; UK-NAMN = UK National Ammonia Monitoring Network

using a similar filter pack as CAPMoN, but operated at 1.5 lpm for eastern U.S. sites and 3.0 lpm for western U.S. sites. The EU-NitroEurope and UK Acid Gas and Aerosol Network (AGANet) use similar low-flow (~0.4 lpm) denuder/filter pack systems to collect particles (size cut ~4.5 μm) and gases on monthly schedules. Tubular denuders collect HNO_3, SO_2 and NH_3, followed by a sequence of filters to collect particles plus volatilized NO_3^- and NH_4^+ (Flechard et al., 2011: Tang et al., 2018).

Results show that concentrations of NH_3 and HNO_3 are generally consistent with those reported for background sites in Europe and North America. NH_3 data from 10 studies/networks indicate that annual average concentrations are generally $\leq$0.2 μg m^{-3}, while data from background sites in northern Europe show concentration on the order of 0.1 μg m^{-3} (Fletchard et al., 2011; Ferm and Hellsten, 2012). This is similar to the range observed for remote and central sites in the TEEM network (0.10–0.16 μg m^{-3}).

Results for SO_2 show that concentrations in the AOSR are elevated relative to regional and remote sites in the USA and Europe. Remote sites in the TEEM network show an average concentration of ~1 μg m^{-3}, which is higher than CASTNet sites in the western U.S. (range ~0.2–0.8 μg m^{-3}). Interestingly, data from two CAPMoN sites in British Columbia and Saskatchewan show the same thing; however, the CAPMoN data are from 2010 and may not reflect current (2017) conditions. NO_2 datasets are sparser than the other gases, but available data suggest that concentrations at remote TEEM sites are in line with forested sites in Europe and North America.

3.4. S, N and BC in PM_{10} and $PM_{2.5}$

3.4.1. Spatial patterns

Summary statistics for major ions in PM_{10} at two industrial sites and four community sites are listed in Appendix Table A.9. The sites are ordered from north to south and span roughly 105 km from SMRM to ANZC (see Fig. 1). SO_4^{2-} is the dominant anion at all sites with an average concentration of 0.86 ± 0.09 μg m^{-3} across sites and a gradient of about 30% from north to south. Ca^{2+} is the dominant cation at all sites, except ANZC, with an average concentration of 0.34 ± 0.28 μg m^{-3} across sites and a range in excess of 600%. The other major ions, NH_4^+, K^+ and NO_3^-, exhibit relatively consistent concentrations across sites.

Ion balances for the six PM_{10} monitoring sites are shown in Appendix Figure A.7. As seen for PM_{10}, Ca^{2+} and NH_4^+ are dominant cations and SO_4^{2-} is the dominant anion. Na^+ and Cl^- are minor contributors to the ion balance, except at the two sites in Fort McMurray (PATM and ATRV) where rock salt is used on roads as a de-icing agent in the winter. Comparison of the sum of measured cations (Σcations) and the sum of measured anions (Σanions) shows significant imbalances with excess Σcations at all sites. The imbalance is roughly equivalent to Ca^{2+}, which suggests that much of PM_{10} Ca^{2+} originates as $CaCO_3$ and that CO_3^{2-} and/or HCO_3^- is the missing anion. This is consistent with the use of crushed limestone for construction of mine roads and haul roads throughout the region.

The ionic composition of $PM_{2.5}$ for the community sites (n = 4) and FHM sites (n = 4) is shown in Appendix Figure A.8. Data for the community sites reflect 9-year averages (2009–17), while those for the FHM sites are for 2017 only. NH_4^+ and SO_4^{2-} are the dominant cation and anion, respectively, at all eight sites. Community sites have an excess of cations over anions while FHM sites have excess anions over cations. $PM_{2.5}$ composition therefore makes a fairly rapid transition from net cations to net anions from the river valley community sites to the surrounding forested sites.

Comparison of PM_{10} and $PM_{2.5}$ concentrations at the community sites shows that <5% of NH_4^+, ~15–20% of SO_4^{2-} and >50% of Ca^{2+}, Mg^{2+}, Na^+ and Cl^- are found in coarse PM (see Appendix Figure A.9). The near absence of NH_4^+ in $PM_{10\text{-}2.5}$ indicates that most of the SO_4^{2-} is chemically associated with another cation, and may be formed heterogeneously, such as *via* reaction between SO_2 and alkaline PM, or during occasional fog/ice fog events in the river valley. Additional size distribution data (e.g., via multi-stage impactor) are needed to better define chemical associations and coarse particle deposition rates.

Monthly average concentrations of major ions in PM_{10} show two distinct patterns over the course of the year (Fig. 4). NH_4^+, SO_4^{2-} and NO_3^- are generally highest in winter and decrease from winter to early fall. The monthly pattern for Ca^{2+} (and Mg^{2+}, not shown) is almost a mirror image of the other major ions. Lowest average concentrations occur from December through February and highest from March through August, with a factor of ~5 overall range. Landis et al. (2017a) also observed this pattern for PM samples collected at Fort McKay during 2010–2011.

Wind speed is a key variable in the suspension/resuspension of surface particulate matter (Wang et al., 2015). Meteorological data from regional sites shows that average wind speed is typically lowest from December through February and highest from March through May. The monthly pattern of Ca^{2+} and other base cations may be controlled by the combination of snow cover/frozen ground and low wind speeds in winter, followed by thawing/drying of soils and higher wind speeds in spring and summer.

Linear regressions of annual average PM_{10} components versus year show mostly non-significant ($p \sim 0.1$–0.3) trends for 2009–2017 (Appendix Table A.10). Exceptions to this include NH_4^+ (significant negative slope at all sites except PATM), and SO_4^{2-} (significant negative slope at ANZC only). Similar to SO_2 and NO_2, most slopes are negative and correspond to concentration decreases of a few % per year; however, the data record is insufficient determination statistically significant trends. Aas et al. (2019) noted similar, but statistically significant, rates of decline for aerosol sulfate over Europe and North America from 2000-2015. Feng et al. (2019) reported declines in SO_4^{2-}, NO_3– and NH_4^+ of 73%, 29% and 66%, respectively, across eastern Canada/U.S. from 1990 to 2015; and Tang et al. (2018) reported declines in SO_4^{2-}, NO_3– and NH_4^+ of 69%, 52% and 62%, respectively, across the UK from 1999 to 2015.

The spatial distributions of major ions in $PM_{2.5}$ during 2017 are shown in Appendix Figure A.10. In general, SO_4^{2-}, NO_3^- and NH_4^+ exhibit ranges of about a factor of 2–3, and concentrations are highest at the three community sites in the Athabasca River valley (BGFM, PATM and ATRV) and lowest at the FHM sites 100–125 km to the east and west. Ca^{2+} concentrations show a broader range (factor of 12 +) and are much higher at the community sites. Small differences between the westernmost, northernmost and easternmost forest health sites may reflect upwind/downwind effects surrounding the oil sand production operations.

3.4.2. Comparison with literature values for NH_4^+, NO_3^- and non-sea salt SO_4^{2-}

TEEM data for $PM_{2.5}$ NH_4^+, NO_3^- and non-sea salt SO_4^{2-} ($nssSO_4^{2-}$) are compared with literature values in Table 2. $nssSO_4^{2-}$ is used instead of measured SO_4^{2-} to avoid positive biases at coastal or near-coastal sites with high concentrations of sea salt PM (SO_4^{2-}: Na^+ in bulk seawater ~0.25) (Keene et al., 1986). The difference between $nssSO_4^{2-}$ and SO_4^{2-} at TEEM sites, and many inland sites, is $\leq$2%, but differences in the U.K., for example, have been shown to be as high as 83% (Tang et al., 2018). Also shown in Table 2 are t-NH_4^+ (i.e., NH_3 + NH_4^+, expressed as NH_4^+) and t-NO_3^- (HNO_3 and NO_3^-, expressed as NO_3^-). These are included, where possible, because totals may be more representative when comparing data across several different techniques. Measurement approaches for CAPMoN, CASTNet and AGANet were described previously. For the U.S. Interagency Monitoring of Protected Visual Environments

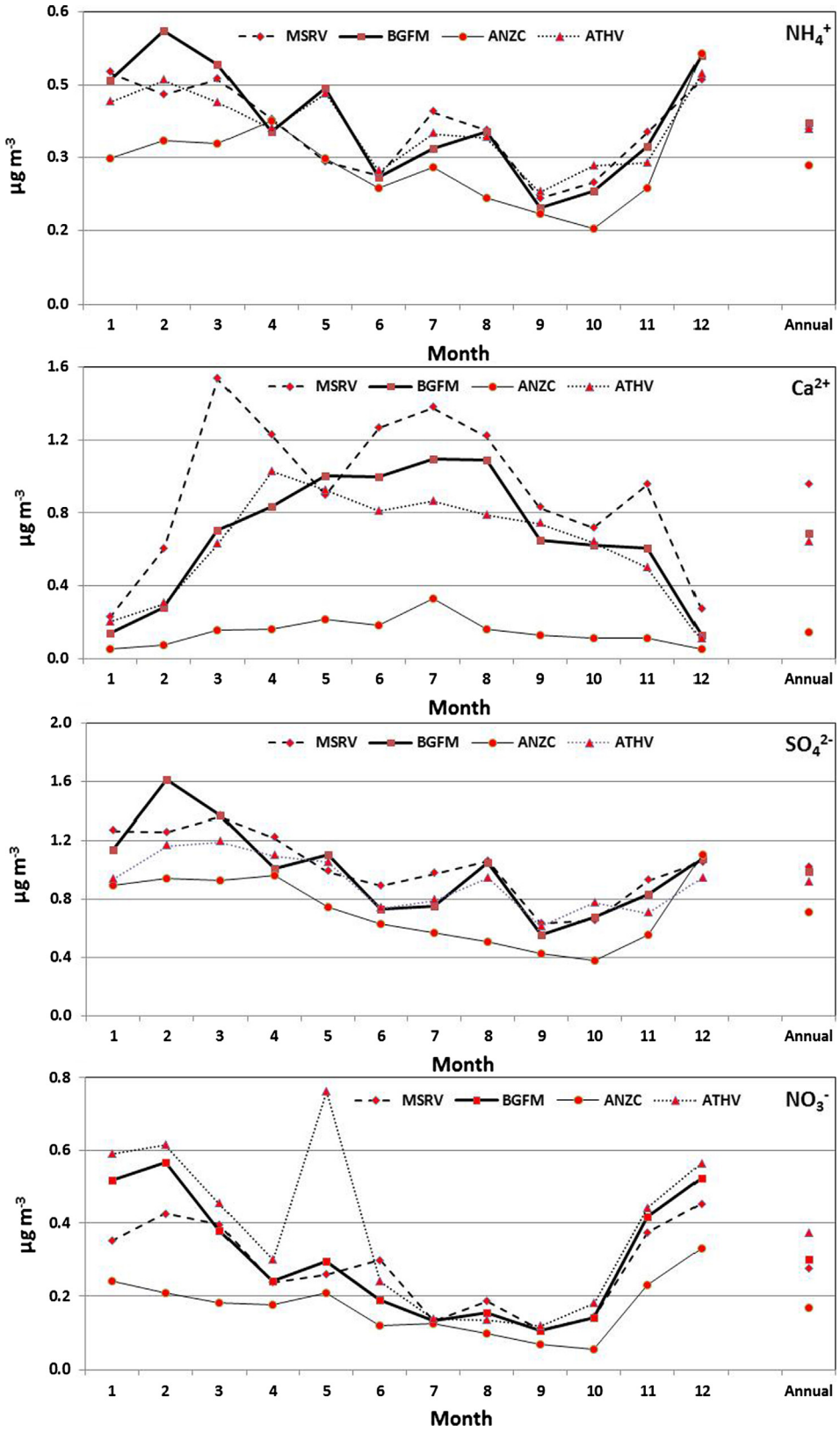

Fig. 4. Monthly mean PM_{10} NH_4^+, Ca^{2+}, SO_4^{2-} and NO_3^- at an industrial site (MSRV) and three community sites (BGFM, ATHV and ANZC).

(IMPROVE) network, $PM_{2.5}$ samples (following removal of HNO_3 andSO_2) are collected on nylon filters every third day and analyzed for SO_4^{2-} and NO_3^- (Malm et al., 1994).

NH_4^+ and NO_3^-concentrations show roughly a factor of 10 range within each network (factor of 6 for CAPMoN), with minimum values ~0.1–0.2 μg m^{-3} and maximum values ~1–2 μg m^{-3}. The two

Table 2
Comparison of TEEM $PM_{2.5}N$ & non-sea salt S with literature values.

Location (Program)	Meas. Period	Method	PM fraction	Setting	Concentration (μg m^{-3})					Ref.
					NH_4^+	NO_3^-	$nssSO_4^{2-}$	t-NH_4^+	t-NO_3-	
AOSR, CA (WBEA-TEEM)	2017	TF	2.5	community (n = 4)	0.20–0.34	0.07–0.19	0.54–0.88	n.m.	n.m.	this study
AOSR, CA	2017	FP	"	remote (n = 3)	0.09–0.13	0.07–0.14	0.32–0.41	0.14–0.24	0.24–0.65	"
AOSR, CA		"	"	central (n = 1)	0.20	0.14	0.57	0.39	0.61	"
Saturna, BC, CA (ECCC-CAPMoN)	2010	FP	open	regional	0.22	0.55	0.64	n.m.	1.2	CAPMoN, 2019
Bratt's Lake, SK, CA	"	"	"	"	0.56	0.97	1.1	n.m.	1.5	"
E. CA	"	"	"	regional (n = 12)	0.19–1.1	0.13–1.9	0.64–2.1	n.m.	0.23–2.7	"
E. USA (USEPA-CASTNet)	2017	FP	open	regional (n = 54)	0.18–0.75	0.18–1.5	0.50–1.7	n.m.	0.37–2.4	CASTNet, 2019
W. USA	"	"	"	regional (n = 32)	0.12–0.54	0.10–1.2	0.27–1.4	n.m.	0.25–2.5	"
Alaska, USA	"	"	"	regional (n = 1)	0.09	0.05	0.27	n.m.	0.11	"
E. USA (IMPROVE)	2017	NF	2.5	regional (n = 32)	n.m.	0.13–1.2	0.52–1.3	n.m.	n.m.	IMPROVE, 2019
W. USA (")	"	NF	"	regional (n = 32)	n.m.	0.06–1.0	0.22–1.3	n.m.	n.m.	"
Alaska, USA (")	"	NF	"	regional (n = 4)	n.m.	0.04–0.09	0.24–0.47	n.m.	n.m.	"
Europe (EU-Nitro Europe IP)	2007–08	FP	open	forest (n = 29)	0.15–1.7	0.09–4.4	n.m.	0.32–6.7	0.27–5.9	Flechard et al., 2011
UK (UK-AGANET)	2015	FP	~4.5	rural bgnd. (n = 28)	0.13–0.94	0.40–1.8	0.10–0.50	0.20–6.8	0.48–2.3	AGANET, 2019

TF = Teflon filter; FP = Teflon + Nylon filters; NF = nylon filter; n.m. = not measured
IMPROVE = Interagency Monitoring of Protected Visual Environments

exceptions to this are Europe with a maximum NO_3^- concentration of 4.4 μg m^{-3} and the UK with a minimum NO_3^- concentration of 0.4 μg m^{-3}. Results for the AOSR show that $NH4^+$ and NO_3^- at remote sites correspond to the low end of observations from CA, USA, UK and Europe, while those from central and community sites are 2–3 times higher.

For $nssSO_4^{2-}$, concentrations show a factor of five range within each network and an overall range of 0.1 μg m^{-3} for the northern UK to 1.7 μg m^{-3} for the eastern U.S. and eastern Canada. Data for Alaska and the westernmost sites in the continental U.S. suggest fairly consistent values of 0.26 ± 0.03 μg m^{-3}. Using this as a pint of comparison, concentrations at remote, central and community sites in the AOSR are roughly 1.3, 2 and 2.5 times higher, respectively.

3.5. Deposition of S, N and BC

3.5.1. IER deposition data

Annualized (2011–2012) bulk NH_4^+-N, bulk NO_3^--N and throughfall SO_4^{2-}-S deposition are summarized in Appendix Table A.11 for 20 sites with ≥3 years of data. A valid year is defined herein as one that includes consecutive warm and cold seasons that together represent 10–14 months of deposition. Mean bulk NH_4^+-N deposition varies across the domain by almost a factor of 3. Mean loadings ≥1.2 kg-N ha^{-1} a^{-1} are observed at 5 sites located near oil sand operations and within or immediately adjacent to the Athabasca River valley. Mean loadings ≤0.8 kg-N ha^{-1} a^{-1} occur at several remote sites near the northern, western and southern extremes of the network. Bulk NO_3^--N deposition is roughly 50% of bulk NH_4^+-N deposition at most sites and follows a similar pattern. Mean loadings ≥1 kg-N ha^{-1} a^{-1} and ≤0.5 kg-N ha^{-1} a^{-1} are observed at 3 central sites and 9 remote sites, respectively. Throughfall loadings of SO_4^{2-}-S are higher than bulk N deposition and vary by almost a factor of 20 across sites. Mean SO_4^{2-}-S deposition is ≥ 10 kg-S ha^{-1} a^{-1} at four central sites and ≤ 2 kg-N ha^{-1}-a^{-1} at six remote sites.

Bulk NH_4^+-N deposition, bulk NO_3^--N deposition and throughfall SO_4^{2-}-S deposition averaged over 2 time periods: 2008–2012 and 2013–17 are presented in Appendix Figure A.11. Average deposition for bulk NH_4^+-N and bulk NO_3^--N are generally similar across time periods. In contrast, throughfall SO_4^{2-}-S deposition data suggest decreases for four remote sites (1001, 2001, 2010 and 2013) and stable, but much higher, deposition for three central sites. Decreases from the earlier to later time periods are statistically significant only for sites 2001 and 2013. Relatively strong inter-site correlations (r^2 = 0.6–0.9) for bulk N components and throughfall S indicate that sites vary more or less together over time. In other words, regional or synoptic conditions (e.g., precipitation amount/type, etc.) cause deposition to increase or decrease from year to year, but without dramatically changing the overall spatial pattern.

IER throughfall data for BC are summarized in Appendix Table A.12. There are fewer sites and a shorter period of record for BC than for N and S deposition. The time series is also discontinuous, as described previously. Nevertheless, results show striking inter-annual variability. Focusing on Ca^{2+}, the dominant BC, annual deposition in 2009 varied by roughly a factor of four across sites. Ca^{2+} deposition was 5–9 kg ha^{-1} a^{-1}at three near field sites (1004, 2054 and 2012), and < 2.5 kg ha^{-1} a^{-1} at two remote sites far to the west and east of operations (2001 and 2013, respectively). For the 2014–16 period, Ca^{2+} was 4–10 times higher at the two remaining near field sites, but still in the range of 2–3 kg ha^{-1} a^{-1} at several remote sites. The one exception to this was site 2010, which experienced very high deposition in 2015–16, possibly related to the Horse River Wildfire. The timing of elevated Ca^{2+} deposition at near field sites can be explained, at least in part, by nearby (1–3 km) highway construction activities.

Deposition versus distance curves for bulk NH_4^+-N, bulk NO_3^--N, throughfall SO_4^{2-}-S and throughfall Ca^{2+} are shown in Fig. 5. N and S deposition are plotted as a function of distance to the nearest stack, while Ca^{2+} is plotted as a function of distance to the center of the nearest mining operation. The latter approach is based on findings of Landis et al. (2017b, 2019) who identified surface oil sand production operations as a major source of Ca^{2+} and other crustal elements in PM collected at Fort McKay and in lichen samples collected throughout the region. Steep declines in deposition with increasing distance are apparent for all four components, and a reasonable fit can be produced with a simple inverse-distance regression curve (r^2 = 0.45–0.97). These inverse-distance curves suggest three spatial domains surrounding oil sand activities: a source-dominated domain from the origin to a distance of about 10–20 km; a transition domain extending out to 40–80 km and a "background" dominated domain further afield. This is consistent with lichen biomonitoring results (Landis et al., 2019), but is uncertain because there are no throughfall measurements for BC between 12 km and 50 km, and only a single measurement for S and N in this range.

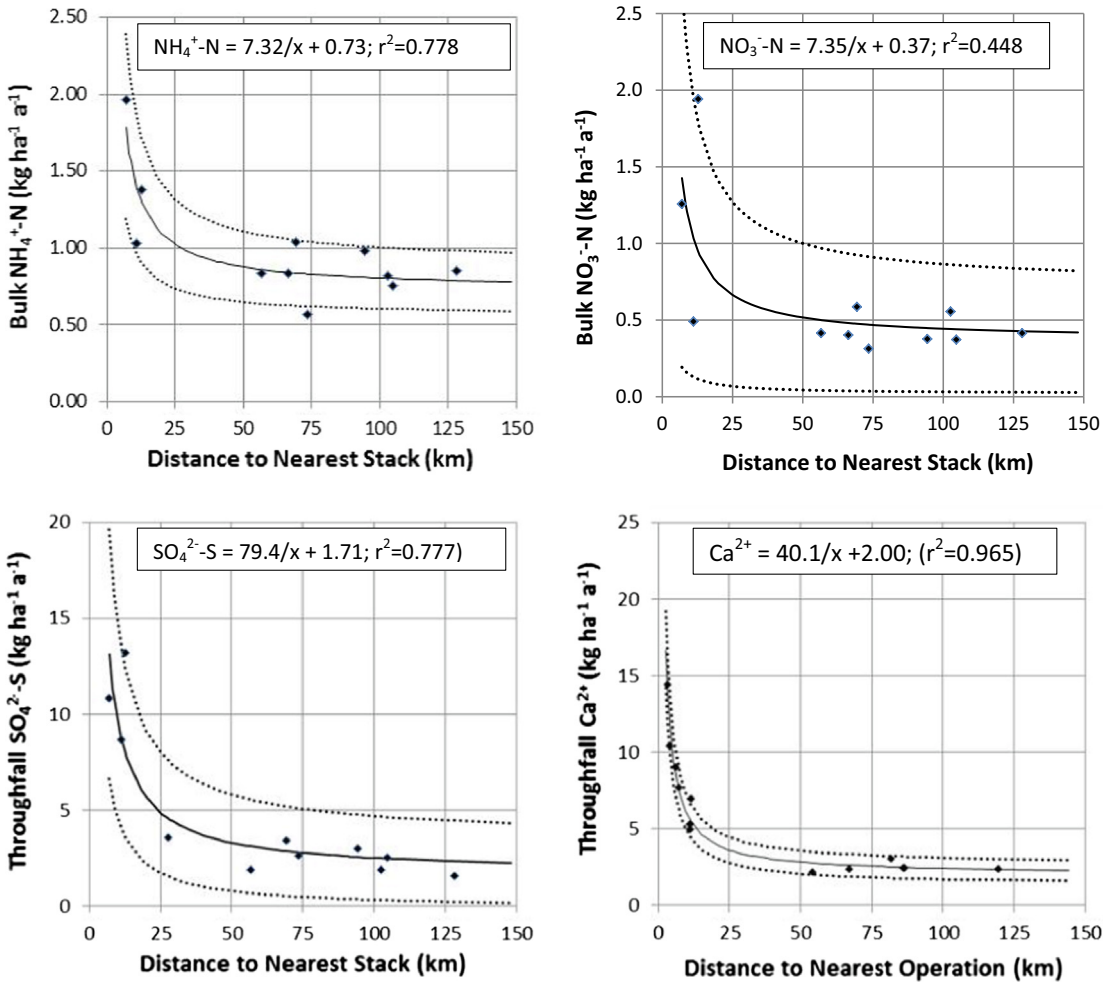

Fig. 5. Deposition vs. distance curves for bulk NH_4^+-N, bulk NO_3^--N, throughfall SO_4^{2-}-S and throughfall Ca^{2+}. Dashed lines represent 95% confidence intervals.

3.5.2. Ndep Sdep, BCdep and PAI at FHM sites

Estimated Ndep is shown by site and component in Fig. 6, with sites arranged from west to east to provide a cross-section of the AOSR. Ndep ranges from 5.7 kg-N ha^{-1} a^{-1} at site 2012 to slightly < 2 kg-N ha^{-1} a^{-1} at several remote sites. Total deposition exceeds 3 kg-N ha^{-1} a^{-1} at 10 sites and 4 kg-N ha^{-1} a^{-1} at 5 central sites. Except for dry NO_2-N, the percent contribution of individual components to Ndep varies by about a factor of 2 across the region: bulk NH_4-N (24–41%), bulk NO_3-N (17–24%), dry NO_2-N (8–42%), dry HNO_3-N (8–17%), dry NH_3-N (5–12%), dry pNO_3-N (2–4%) and dry pNH_4-N (1–3%). For the centrally located sites, deposition estimates rank as follows: dry NO_2-N ≥ bulk NH_4-N > bulk NO_3-N > dry NH_3-N > dry HNO_3-N > dry pNO_3-N > dry pNH_4-N. At the most distant sites the order of contributions was: bulk NH_4-N > bulk NO_3-N > dry HNO_3-N ≥ dry NO_2-N > dry NH_3-N > dry pNO_3-N > dry pNH_4-N.

Dry deposition of pNO_3-N is underestimated due to lack of PM_{10} data at regional sites. Zhang et al. (2009) measured size distributions of NO_3^- at eight sites across southeastern Canada and showed that 10–77% resided in the > $PM_{2.5}$ size fraction, and varied as a function of site characteristics (e.g., polluted versus remote) and season. The contribution of pNO_3-N deserves further investigation, but an underestimate of a factor of 2 would not appreciably alter total deposition estimates nor would it affect the above rankings of components. This issue does not arise with dry pNH_4^+-N because almost all NH_4^+ is found in the $PM_{2.5}$ fraction.

Reduced N (i.e., dry NH_3 deposition plus bulk NH_4^+ deposition) accounts for 28–58% of Ndep and this percentage generally increases from central sites (i.e., where dry NO_2 dominates) to remote sites. However, Fenn et al. (2015) noted that reduced N deposition significantly exceeded oxidized N deposition at industrial sites very close to operations. Bulk NH_4^+ and bulk NO_3^- together represent 40–62% of Ndep and this percentage increases with distance to operations. In other words, wet and dry processes contribute more or less equally to Ndep in the AOSR.

The current Ndep estimates for FHM sites are roughly half of those reported by Zhang et al. (2009) for eight sites in a west-east transect across Canada from Chalk River, Ontario to Kejimkujik, Nova Scotia (4–10 kg-N ha^{-1} a^{-1} versus <2–6 kg-N ha^{-1} a^{-1}). However, the relative contribution of components followed a similar order with wet NH_4^+-N ≥ wet NO_3-N > NO_2 ~ HNO_3 > NH_3 > pNO_3^-, pNH_4^+.

The current Ndep estimates do not include organic forms of nitrogen (ON) that are known to occur in precipitation, gases and PM (Cornell, 2011). Cape et al. (2012) measured ON in wet deposition at 18 sites across Europe and found that ON deposition ranged from 0.15 to 1.74 kg-N ha^{-1} a^{-1} and contributed 2–36% (median 10%) of dissolved N deposition on an annual basis. Zhang et al. (2009) measured gas phase oxidized ON and estimated dry deposition rates for ON at eight sites across southeastern Canada. Results showed ON deposition to be ≤ 0.75 kg-N ha^{-1} a^{-1} for "polluted" sites, ≤0.25 kg-N ha^{-1} a^{-1} for "less polluted" sites and ≤ 0.1 kg-N

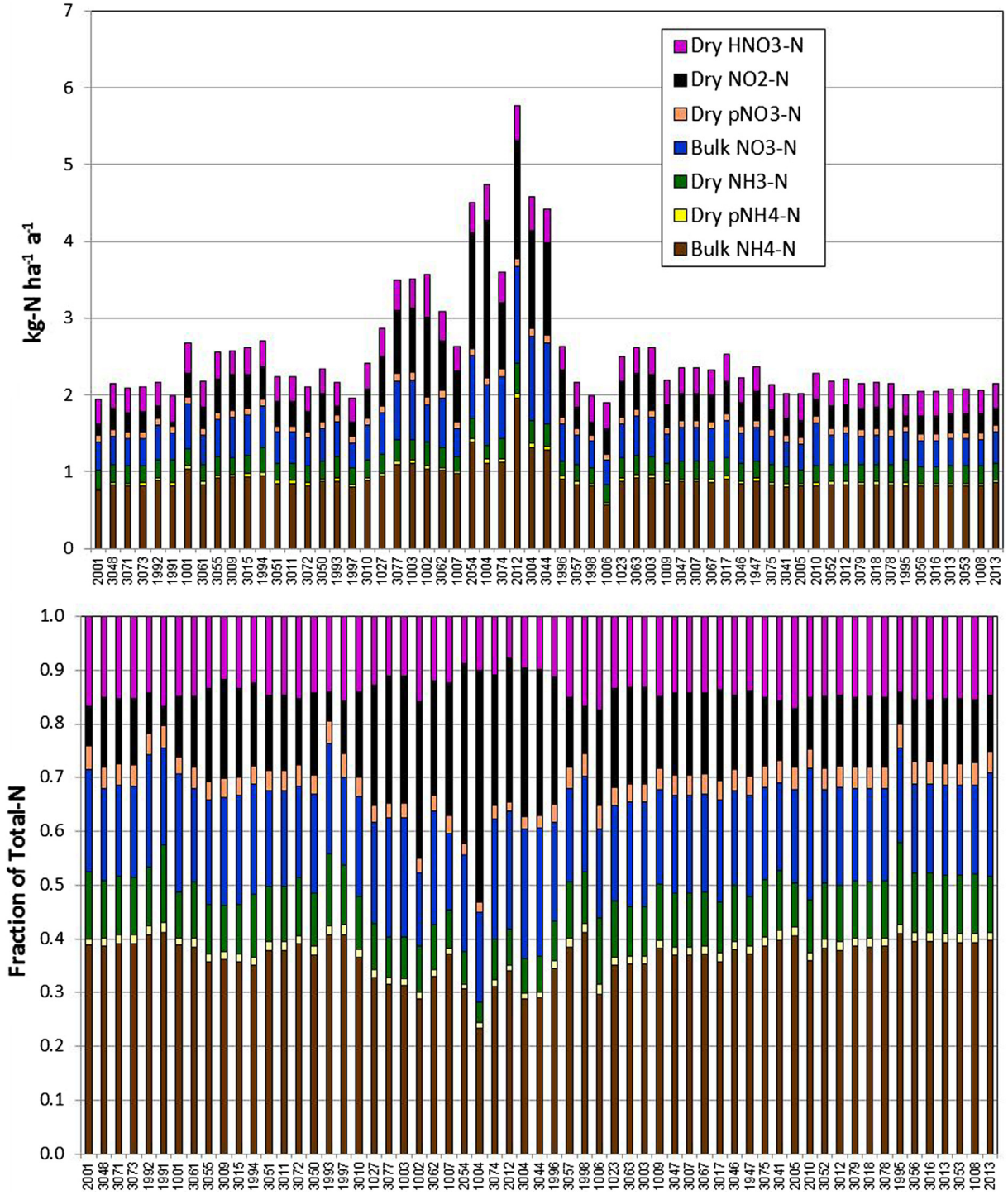

Fig. 6. Estimated 2011–2012 components of Total-Nitrogen (Total-N) deposition to TEEM sites. Absolute deposition in upper panel and relative contributions in lower panel. Sites are arranged west to east on the x-axis.

ha^{-1} a^{-1} for "clean" sites. Data also suggest that ON can represent a significant fraction (10–33%) of total N in $PM_{2.5}$ (Zhang et al., 2002; Lin et al., 2010; Rastogi, et al., 2011: Matsumoto et al., 2019). If aerosol ON is primarily in the $PM_{2.5}$ fraction, then the contribution of ON dry deposition to Ndep is likely <5%. However, little is known about ON in larger size fractions, and therefore particulate ON deposition could be important. Further research is needed to understand atmospheric concentrations, sources and effects of ON in the AOSR.

Comparison of Ndep and throughfall N deposition ($Ndep_{TF}$) for 9 sites with Ndep in the range of 2 to 6 kg N ha^{-1} a^{-1} shows that $Ndep_{TF}$ accounts for about 42%–85% of Ndep (see Appendix Figure A.12) and clearly indicates that canopy consumption of atmospheric N is affecting throughfall measurements. The difference between the two fluxes suggests nearly constant canopy uptake of 1.1 ± 0.5 kg N ha^{-1} a^{-1}. If canopy uptake of atmospheric N is constant across the AOSR deposition gradient, then $Ndep_{TF}$ or an adjusted form of $Ndep_{TF}$ may serve as a useful surrogate for

Ndep in areas of high deposition or at sites lacking inputs to drive dry deposition calculations. This is analogous to the treatment of throughfall K^+ and Mg^{2+} for BC estimates.

Estimated Sdep and BCdep are displayed by site in Fig. 7. The pattern for Sdep is similar to Ndep, with maximum deposition near the center of the domain, but with a broader range of deposition. Sdep is <2 kg-S ha^{-1} a^{-1} at 3 remote sites and >6 kg-S ha^{-1} a^{-1} at 10 central sites. Ca^{2+} is the dominant BC, followed by adjusted K^+, adjusted Mg^{2+} and Na^+. In contrast to Ndep and Sdep, BC shows two peaks of elevated deposition. One of the peaks coincides with maximum Sdep and Ndep, and the second peak occurs east and north of the first and includes the three sites with highest BC deposition. Individual components of deposition at FHM sites are listed in Appendix Table A.7.

Estimated PAI for FHM sites is mostly in the range of 0.1–0.2 k eq ha^{-1} a^{-1} (see Fig. 8). The extreme western edge of the domain

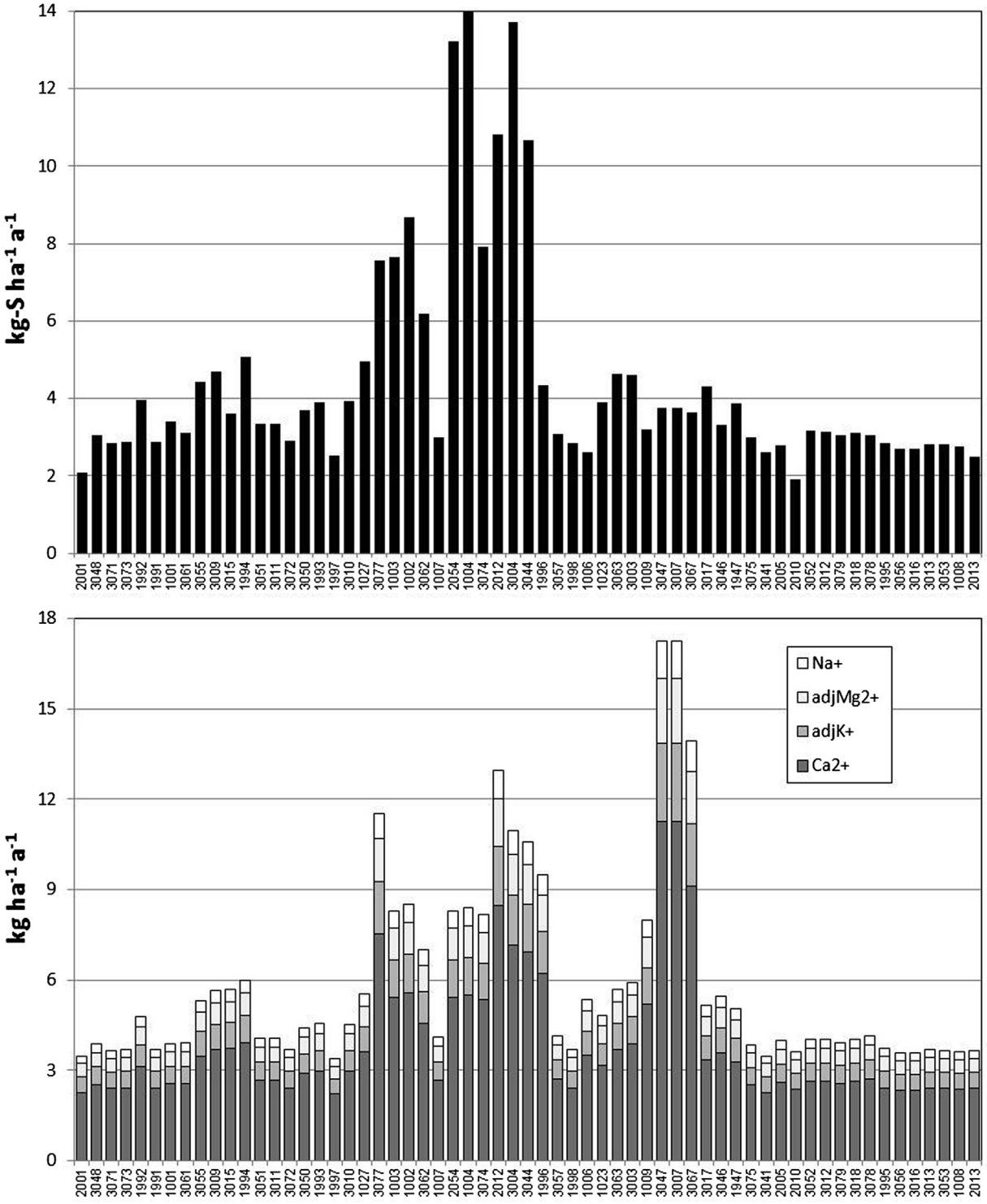

Fig. 7. Estimated 2011–2012 deposition of Total-Sulfur (above) and individual base cations (below). Sites are arranged west to east on the x-axis.

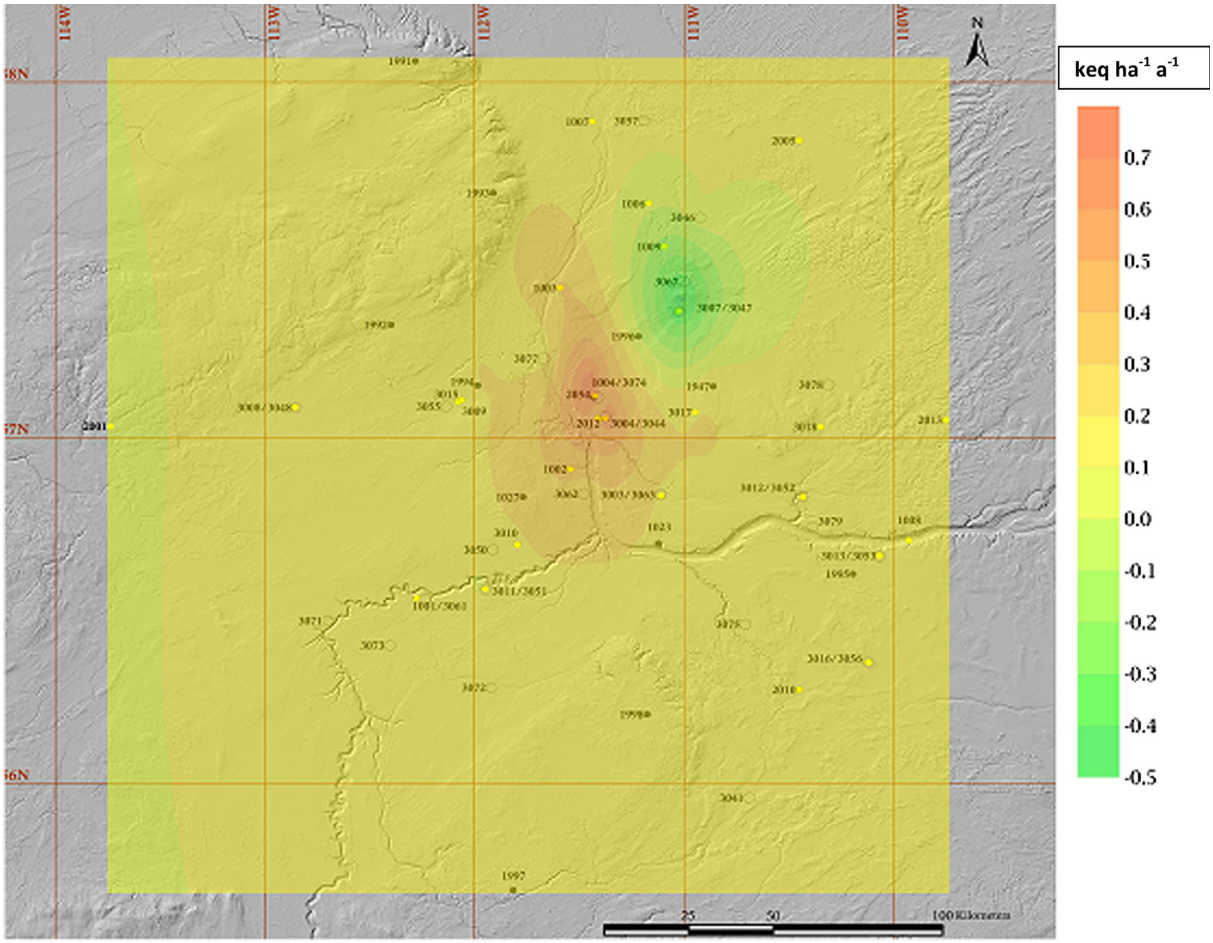

Fig. 8. Estimated 2011–2012 potential acid input (PAI) for TEEM monitoring sites.

exhibits PAI values of 0–0.1 keq ha^{-1} a^{-1}, and there are two distinct areas of significantly positive and zero to negative PAI. The area of highest PAI includes values of 0.3 to 0.7 keq ha^{-1} a^{-1}. It is centered slightly east of the center of oil sands operations and extends roughly 50 km north–south and 25 km east–west. The area of lowest PAI includes values of 0.0 to −0.5 keq ha^{-1} a^{-1} and is located 50 km northeast of the center of operations. The overall pattern shows slightly positive (acidifying) values in those parts of the domain with low Sdep, Ndep and BCdep, and much more positive values near the center of the domain with highest Sdep, Ndep and BCdep. Negative or near-zero PAI values are suggested where there are sources of BC (mines and other surface operations) in areas with moderate to low Sdep and Ndep. Watmaugh et al. (2014) also demonstrated the importance of fugitive dust emissions and BCdep for mitigating acidification across the AOSR.

PAI values for most of the domain are below critical loads for sensitive soils that have been established by the Government of Alberta (Government of Alberta, 2008); that is < 0.25 keq ha^{-1} a^{-1}. Makar et al. (2018) recently estimated that up to 10% of Alberta and portions of Saskatchewan downwind of oil sand production operations exceed critical loads. However, the Makar et al. (2018) analysis was based on significantly different methods for calculating both atmospheric deposition (atmospheric model versus observation-based) and soil sensitivity. Thus, there is a need for further efforts to reconcile approaches for estimating deposition and associated effects across the AOSR. Results of this work will be used in two companion papers that assess impacts of Sdep, Ndep and PAI on soils and vegetation at FHM sites (Bartels et al., 2019; MacKenzie and Dietrich, 2019).

3.5.3. Comparison of TEEM deposition estimates with literature values

TEEM deposition estimates are compared with literature values and publicly available datasets in Table 3. Results must be compared with caution for a number of reasons, including differences in precipitation type and amount across regions and differences in the approach used to estimate dry deposition. For example, annual precipitation in the AOSR is in the range of 400–450 mm per year, which is roughly 50% of that over much of eastern Canada and the U.S., but 100–300% higher than arid parts of the southwestern U.S. Given this range in precipitation, highly variable deposition rates are not surprising.

Results show that bulk deposition at remote TEEM sites is similar to that in the eastern US, eastern CA and NW Europe, but higher than the lowest deposition rates in western CA and US. Bulk NH_4^+ and NO_3^- deposition at central sites is closer to the high end observed for western CA and US, while bulk nss-S is as high or higher than eastern CA and US. For total deposition, remote sites fall towards the low end of reported values for N, nss-S and Ca^{2+}, and central sites fall towards the high end of reported deposition estimates.

Table 3
Comparison of TEEM deposition with literature values.

Location (Program)	Meas. Period	Method	Setting	Wet (or *Bulk*), kg ha^{-1} a^{-1}				Total, kg ha^{-1} a^{-1}			Ref.
				NH_4^+-N	NO_3^--N	nssSO_4^{2-}-S	Ca^{2+}	N	nssS	Ca^{2+}	
AOSR, CA (WBEA-TEEM)	2009–12	B,I	remote (n = 6)	*0.8–1.0*	*0.4–0.6*	*0.8–1.2*	n.r.	1.9–2.1	1.9–2.6	2.3–2.4	this study
		B,I	central (n = 3)	*1.3–2.0*	*1.0–1.3*	*4.6–8.1*	n.r.	4.6–5.8	10.7–14.0	7.5–11.3	"
Esther, AB, CA (CAPMoN)	2009–12	W	regional	1.00	0.62	0.67	0.79	n.r.	n.r.	n.r.	CAPMoN, 2019
W. Canada	2009–12	W	" (n = 3)	0.15–1.5	0.2–1.1	0.27–0.99	0.15–1.2	n.r.	n.r.	n.r.	"
E. CA	2009–12	W	" (n = 24)	0.36–4.0	0.37–2.9	0.52–4.3	0.31–2.5	n.r.	n.r.	n.r.	"
E. Canada	2001–05		rural grass, crops, forest (n = 8)	1.2–4.3	0.5–4.4	n.r.	n.r.	4.3–11	n.r.	n.r.	Zhang et al., 2009
So. Ontario	2010–11	W,I	rural-forested and rural-ag. (n = 7)	3.0–3.4	3.1–3.6	n.r.	n.r.	9.3–16.	n.r	n.r	Zbieranowski and Aherne, 2012
E. USA (USEPA-CASTNet)	2009–12	W,H	regional (n = 54)	1.0–4.2	0.6–2.4	0.6–4.2	0.5–3.9	2.9–16	1.9–10	0.8–10	CASTNet, 2019
W. USA (USEPA-CASTNet)	2009–12	W,H	regional (n = 32)	0.1–3.1	0.1–1.7	0.1–2.1	0.1–4.0	1.9–11	0.4–2.6	0.5–11	"
Grand Tetons N.P., USA	2011	W,I	rural-montane	n.r.	n.r.	n.r.	n.r.	2.2–2.5	n.r.	n.r.	Benedict et al., 2013
NE. Europe (EMEP)	2009–12	W	rural (n = 8)	1.1–3.5	1.0–3.1	1.0–2.0	n.r.	n.r.	n.r.	n.r.	EMEP, 2019
Switzerland	2014	B,I	forest- Central Alps	n.r.	n.r.	n.r.	n.r.	5.0–25	n.r.	n.r.	Thimonier et al., 2019
Denmark	2008	W,M	natural, semi-natural	n.r.	n.r.	n.r.	n.r.	7.0–31	n.r.	n.r.	Hertel et al. 2013
China	2006–2014	W,M	background	1.00	0.50	n.r.	n.r.	2.9	n.r.	n.r.	Xu et al., 2015

B = bulk precipitation; W = wet-only precipitation, I = inferred dry with measured gases/particles; M = modeled dry; n.r. = not reported.
EMEP = European Monitoring and Evaluation Programme.

4. Conclusions

Passive data from air and deposition networks operated by the WBEA TEEM program provide useful data for evaluation of spatial variability and temporal trends, and estimates of S, N, BC and PAI deposition to FHM jack pine sites.

Ambient SO_2 and NO_2 show large (factor of 5–20) spatial gradients with highest concentrations near oil sand operations and lowest concentration at the extremes of the network. Annual average SO_2 concentrations decreased significantly, and more or less linearly, across the AOSR since 2000. NO_2 concentrations showed few significant trends, but generally increased from 2000 to 2009 or 2010, then returned to near-2000 levels by 2017. HNO_3 concentrations vary by a factor of 2–3 across the domain and have been relatively consistent over time. NH_3 concentrations vary by roughly a factor of 6, and show dramatic, site-specific influence from the 2016 Horse River wild fire, and wild fires in previous years. Concentrations of NH_3 and HNO_3 at TEEM sites are near the low end of those reported by networks in Canada, the U.S. and Europe. In contrast, SO_2 concentrations at TEEM sites are higher than rural/remote sites in the western U.S. and similar to sites in the eastern U.S and eastern Canada.

$PM_{2.5}$ and PM_{10} data are relatively limited and additional sites upwind and downwind of sources are needed to understand spatial patterns. The coarse fraction ($PM_{10\text{-}2.5}$) at industrial and community sites accounts for a large percentage of BC and ion balances show significant alkalinity. The fine fraction ($PM_{2.5}$) accounts for the majority of NH_4^+, SO_4^{2-} and NO_3^- at community sites. Ion balances for $PM_{2.5}$ show excess cations at community sites, but excess anions at FHM sites. PM_{10} data show striking seasonality with highest NH_4^+, SO_4^{2-} and NO_3^- during the winter and highest Ca^{2+} during spring and summer. Like NH_3, surface emissions of Ca^{2+} may be considerably reduced by snow cover and frozen ground. Local limestone quarrying and crushing operations are also suspended during the winter, thereby temporarily eliminating a potentially significant source of Ca^{2+}. Trend analyses suggest that most components of PM_{10} are declining at WBEA sites, but the only significant ($p < 0.05$) trends are for NH_4^+ (all sites) and SO_4^{2-} (1 site). $PM_{2.5}$ concentrations of NH_4^+ and NO_3^- at remote TEEM sites are similar to the lowest concentrations reported for Canada, the U.S. and Europe.

Canopy uptake reduces throughfall deposition of NH_4^+ and NO_3^- to FHM jack pine sites by about 1 kg-N ha^{-1} a^{-1}. As a result, bulk deposition is combined with modelled dry deposition of nitrogenous gases and particles to obtain estimates of Ndep. In contrast, the jack pine canopy contributes significantly to throughfall deposition of K^+ and Mg^{2+} and measured loadings must be adjusted downward for calculating BCdep and PAI. Further research is needed to better understand canopy exchanges in TEEM jack pine stands and to guide interpretation of throughfall measurements (especially BCdep). High (±50%) year to year variability of Sdep, Ndep and BCdep highlights the need for long-term monitoring to evaluate trends and impacts from new development.

Estimated Ndep and Sdep at FHM sites were ~2.0–5.7 kg-N ha^{-1}-a^{-1} and ~2.0–14 kg-S ha^{-1} a^{-1}, respectively. Bulk deposition of NH_4^+-N and NO_3^--N accounted for > 40% of total-N deposition networkwide. Dry deposition calculations showed that NO_2 was dominant at sites close to operations, but that HNO_3, NO_2 and to a lesser extent NH_3, contributed similarly to dry deposition at remote sites. Dry NH_3 deposition and dry HNO_3 deposition were as least a factor of 2 lower than previously estimated for the AOSR (Hsu et al., 2016). This can be explained by changes in the passive sampler collection substrates, blank-correction and adjustments that were performed to correct a previous calculation error (NH_3 only).

Deposition gradients around sources were reasonably well explained ($r^2 > 0.4$) by a simple inverse distance relationship between receptor sites and sources. Sdep, Ndep and BCdep at near field sites within 10–15 km of sources were high and variable. Sdep, Ndep and BCdep at remote sites $\geq$ 50 km from sources were low and relatively constant, suggesting that deposition at this distance approached regional values.

PAI estimates showed net acidic deposition for 2011–2012 to be in the range of 0.1–0.2 keq ha^{-1} a^{-1} for the majority of sites. Higher values (0.3–0.7 keq ha^{-1} a^{-1}) were predicted near the center of oil sand operations, while negative values (net alkalinity) were predicted in an area of relatively new surface mining activity northeast of Fort McKay. These negative PAI values are driven to a large extent by the spatial interpolation approach used to estimate BC deposition. Results are consistent with spatial patterns for lichen biomonitoring samples collected between 2008 and 2017 (Landis et al., 2019), but should be confirmed by actual measurements.

Declaration of Competing Interest

The authors declare that there is no conflict of interest regarding the publication of this article.

Acknowledgements

Funding for this work was provided from the Wood Buffalo Environmental Association (WBEA), Fort McMurray, AB, Canada contract T107-17 through support from the Oil Sands Monitoring Program (OSM). The content and opinions expressed by the authors in this document do not necessarily reflect the views of the Wood Buffalo Environmental Association (WBEA) or of the WBEA membership. The efforts of Cody David, Gary Cross, Melissa Dube, Hayley Drake, Tyler Tracksell and Kendra Thomas in maintaining the TEEM networks and continuous air quality monitoring stations are greatly appreciated. The author(s) acknowledge Environment and Climate Change Canada for the provision of chemistry data from the Canadian Air and Precipitation Monitoring Network accessed from the Government of Canada Open Government Portal at open.canada.ca.

Appendix A. Supplementary data

Supplementary data to this article can be found online at https://doi.org/10.1016/j.scitotenv.2019.134864.

References

Aas, W. et al., 2019. Global and regional trends of atmospheric sulfur. Sci. Rep. 9 (953).
Addison, P.A., Puckett, K.J., 1980. Deposition of atmospheric pollutants as measured by lichen element content in the Athabasca oil sands area. Can. J. Bot. 58, 2323–2334.
Bari, M.A., Kindzierski, W.B., Spink, D., 2016. Twelve-year trends in ambient concentrations of volatile organic compounds in a community of the Alberta Oil Sands Region. Canada. Environ. Int. 91, 40–50.
Barrie, L.A., Kovalick, J.A., 1980. Wintertime Investigation of the Deposition of Pollutants around an Isolated Power Plant in Northern Alberta. Prepared for the Alberta Oil Sands Environmental Research Program by Atmospheric Environment Service, AOSERP Report No. 90:1-115.
Bartels, S.F., Gendreau-Berthiaume, B., Macdonald, S.E., 2019. The impact of atmospheric acid deposition on tree growth and forest understory vegetation in the Athabasca oil sands region. (this issue).
Benedict, K., Chen, X., Sullivan, A., Li, Y., Day, D., Prenni, A., Levin, E., Kreidenweis, S., Malm, W., Schichtel, B., Collett, J., 2013. Atmospheric concentrations and deposition of reactive nitrogen in Grand Teton National Park. J. Geophys. Res. Atmos. 118 (20), 11875–11887.
Cape, J.N., Tang, Y.S., Gonzalez-Benitez, J., Makkonen, U., Jocher, M., Stolk, A., 2012. Organic nitrogen in precipitation across Europe. Biogeosci. Discuss. 9, 8093–8109.
CASTNet, 2019. U.S. Environmental Protection Agency Clean Air Markets Division Clean Air Status and Trends Network (CASTNET), Annual Total Deposition Table, www.epa.gov/castnet. Date accessed: September 12, 2019.
Chen, X., Day, D., Schichtel, B., Malm, W., Matzoll, A., Mojica, J., McDade, C., Hardison, E., Hardison, D., Walters, S., Van De Water, M., Collett, J., 2014. Seasonal ambient ammonia and ammonium concentrations in a pilot IMPROVE NHx monitoring network in the western United States. Atmos. Environ. 91, 118–126.
Cornell, S.E., 2011. Atmospheric nitrogen deposition: revisiting the question of the importance of the organic component. Environ. Pollut. 159, 2214–2222.
Davidson, C., Spink, D., 2018. Alternate approaches for assessing impacts of oil sands development on air quality: a case study using the First Nation Community of Fort McKay. J. Air Waste Manag. Assoc. 68, 308–328.
Davies, M.J.E., 2012. Air quality modeling in the Athabasca Oil Sands Region. In: Alberta Oil Sands: Energy, Industry and the Environment. Elsevier, Oxford, England, pp. 267–309.
Edgerton, E.S., Hartsell, B.E., Saylor, R.D., Jansen, J.J., Hansen, D.A., Hidy, G.M., 2006. The Southeastern Aerosol Research and Characterization Study: Part II. filter-based measurements of fine and coarse particulate matter mass and composition. J. Air Waste Manage. Assoc. 55, 1527–1542.
EMEP, 2019. European Monitoring and Evaluation Program. http://ebas.nilu.no/Default.aspx (see also EMEP description at http://www.atmos-chem-phys.net/12/5447/2012/acp-12-5447-2012.pdf). Date accessed: September 12, 2019.
Environment Canada, 2012. National Air Pollution Surveillance (NAPS) Network Reference Method for the Measurement of PM2.5 Concentration in Ambient Air Using Filter Collection and Gravimetric Mass Determination, Method No.: 8.06/2.0/M. Effective Date: January 4, 2012.
Environment and Climate Change Canada, 2019. Canadian Air and Precipitation Monitoring Network (CAPMoN), Toronto, Ontario, Canada.
Feng, J., Chan, E., Vet, R., 2019. Air quality in the eastern United States and Eastern Canada for 1990–2015: 25 years of change in response to emission reductions of SO2 NOx in the region. Atmos. Chem. Phys Discuss.. https://doi.org/10.5194/acp-2019-567 (In review).
Fenn, M.E., Bytnerowicz, A., Schilling, S.L., Ross, C.S., 2015. Atmospheric deposition of nitrogen, sulfur and base cations in jack pine stands in the Athabasca Oil Sands Region, Alberta, Canada. Environ. Pollut. 196, 497–510.
Fenn, M.E., Ross, C.S., Schilling, S.L., Baccus, W.D., Larrabee, M.A., Lofgren, R.A., 2013. Atmospheric deposition of nitrogen and sulfur and preferential canopy consumption of nitrate in forests of the Pacific Northwest, USA. For. Ecol. Manage. 302, 240–253.
Ferm, M., Hellsten, S., 2012. Trends in atmospheric ammonia and particulate ammonium concentrations in Sweden and its causes. Atmos. Environ. 61, 30–39.
Ferm, M., Hultberg, H., 1999. Dry deposition and internal circulation of nitrogen, sulphur and base cations to a coniferous forest. Atmos. Environ. 33, 4421–4430.
Flechard, C.R., Nemitz, E., Smith, R.I., Fowler, D., Vermeulen, A.T., Bleeker, A., Erisman, J.W., Simpson, D., Zhang, L., Tang, Y.S., Sutton, M.A., 2011. Dry deposition of reactive nitrogen to European ecosystems: a comparison of inferential models across the NitroEurope network. Atmos. Chem. Phys. 11, 2703–2728. https://doi.org/10.5194/acp-11-2703-2011.
Foster, K.R., McDonald, K., Eastlick, K., 2001. Development and application of critical, target, and monitoring loads for the management of acid deposition in Alberta, Canada. Water Air Soil Pollut. 1, 135–151.
Foster, K.R., Davidson, C., Spink, D., 2019. Introduction to the virtual special issue: monitoring ecological responses to air quality and deposition in the Athabasca Oil Sands Region: the Wood Buffalo Environmental Association's terrestrial environmental effects monitoring program. Sci. Total Environ. (this issue)
Government of Alberta, 2008. In: Environment, A. (Ed.), Alberta Acid Deposition Management Framework. Government of Alberta, Edmonton, AB.
Government of Alberta, 2014. 2011 acid deposition assessment for Alberta. July 2014. https://open.alberta.ca/dataset/9eddc860-9121-4b0b-a919-a2c7d72badf8/resource/b1b0255d-3a37-4eb5-a728-946e6450959e/download/2014-2011AcidDepositionAssessment-Jul2014.pdf
Guéguen, C., Cuss, C.W., Cho, S., 2016. Snowpack deposition of trace elements in the Athabasca Oil Sands Region, Canada. Chemosphere 153, 447–454.
Hertel, O., Geels, C., Frohn, L., Ellermann, T., Skjøth, C., Løfstrøm, P., Christensen, J., Andersen, H., Peel, R., 2013. Assessing atmospheric nitrogen deposition to natural and semi-natural ecosystems – Experience from Danish studies using the DAMOS. Atmos. Environ. 66, 151–160. https://doi.org/10.1016/j.atmosenv.2012.02.071.
Hsu, Y.-M., 2013a. Trends in passively-measured ozone, nitrogen dioxide and sulfur dioxide concentrations in the Athabasca Oil Sands Region of Alberta, Canada. Aerosol Air Qual. Res. 13, 1448–1463.
Hsu, Y.-M., 2013b. Trends in passively-measured ozone, nitrogen dioxide and sulfur dioxide concentrations in the Athabasca Oil Sands region of Alberta. Canada. Aerosol Air Qual. Res. 13, 1448–1463.
Hsu, Y.-M., Bytnerowicz, A., Fenn, M.E., Percy, K.E., 2016a. Atmospheric dry deposition of sulfur and nitrogen in the Athabasca Oil Sands Region, Alberta, Canada. Sci. Total Environ. 568, 285–295.
Hsu, Y.-M., Bytnerowicz, A., Fenn, M.E., Percy, K.E., 2016b. Nitrogenous and sulfurous air pollution and atmospheric dry deposition in the Athabasca Oil Sands Region, Alberta, Canada. Sci. Total Environ. 568, 285–295.
IMPROVE, 2019. Interagency Monitoring of Protected Visual Environments (IMPROVE) is a collaborative association of state, tribal, and federal agencies, and international partners. US Environmental Protection Agency is the primary funding source, with contracting and research support from the National Park

Service. The Air Quality Group at the University of California, Davis is the central analytical laboratory, with ion analysis provided by Research Triangle Institute, and carbon analysis provided by Desert Research Institute. http://views.cira.colostate.edu/fed/QueryWizard/Default.aspx. Date accessed: September 12, 2019.

Keene, W.C., Pszenny, A.A.P., Galloway, J.N., Hawley, M.E., 1986. Sea salt corrections and interpretation of constitutent ratios in marine precipitation. J. Geophys. Res. 91, 6647–6658.

Kelly, E.N., Schindler, D.W., Hodson, P.V., Short, J.W., Radmanovich, R., Nielsen, C.C., 2010. Oil sands development contributes elements toxic at low concentrations to the Athabasca River and its tributaries. Proc. Natl. Acad. Sci. U.S.A. 107, 16178–16183.

Landis, M.S., Norris, G.A., Williams, R.W., Weinstein, J., 2001. Personal exposures to $PM_{2.5}$ mass and trace elements in Baltimore, MD, USA. Atmos. Environ. 35, 6511–6524.

Landis, M.S., Pancras, J.P., Graney, J.R., Stevens, R.K., Percy, K.E., Krupa, S., 2012. Receptor modeling of epiphytic lichens to elucidate the sources and spatial distribution of inorganic air pollution in the Athabasca Oil Sands Region. In: Percy, K.E. (Ed.), Alberta Oil Sands: Energy, Industry and the Environment. 11. Elsevier, Oxford, England, pp. 427–467.

Landis, M.S., Edgerton, E.S., White, E.M., Wentworth, G.R., Sullivan, A.P., Dillner, A. M., 2017a. The impact of the 2016 Fort McMurray Horse River Wildfire on ambient air pollution levels in the Athabasca Oil Sands Region, Alberta. Canada. Sci. Total Environ. 618, 1665–1676.

Landis, M.S., Pancras, J.P., Graney, J.R., White, E.M., Edgerton, E.S., Legge, A., Percy, K. E., 2017b. Source apportionment of ambient fine and coarse particulate matter at the Fort McKay community site, in the Athabasca Oil Sands Region, Alberta. Canada. Sci. Total Environ. 584–585, 105–117.

Landis, M.S., Studabaker, W., Puckett, K., Pancras, J.P., Graney, J.R., White, E.M., Edgerton, E.S., 2019. Source apportionment of an epiphytic lichen biomonitor to elucidate the sources and spatial distribution of polycyclic aromatic hydrocarbons in the Athabasca Oil Sands Region, Alberta. Canada. Sci. Total Environ. 654, 1241–1257.

Li, Y., Schwandner, F., Sewell, H., Zivkovich, A., Tigges, M., Raja, S., Holcomb, S., Molenar, J., Sherman, L., Archuleta, C., Lee, T., Collett, J., 2014. Observations of ammonia, nitric acid, and fine particles in a rural gas production region. Atmos. Environ. 83, 80–89.

Lin, M., Walker, J., Geron, C., Khlystov, A., 2010. Organic nitrogen in $PM_{2.5}$ aerosol at a forest site in the Southeast US. Atmos. Chem. and Phys. 10, 2145–2157.

Lynam, M.M., Dvonch, J.T., Barres, J.A., Morishita, M., Legge, A., Percy, K., 2015. Oil sands development and its impact on atmospheric wet deposition of air pollutants to the Athabasca Oil Sands Region, Alberta. Canada. Environ. Pollut. 206, 469–478.

Macdonald, E., 2015. Responses of understory vegetation to deposition from oil sand processing operations. In: Clair, T.A., Percy, K.E. (Eds.), Assessing Forest Health in the Athabasca Oil Sands Region. Wood Buffalo Environmental Association, Fort McMurray, Alberta, pp. 134–144.

MacKenzie, M.D., Dietrich, S.T., 2019. Atmospheric deposition in the Athabasca oil sands region has measurable effect on foliar nutrients and soil chemical properties. (this issue).

Makar, P.A., Akingunola, A., Aherne, J., Cole, A.S., Aklilu, Y.-A., Zhang, J., Wong, I., Hayden, K., Li, S.-M., Kirk, J., Scott, K., Moran, M.D., Robichaud, A., Cathcart, H., Baratzedah, P., Pabla, B., Cheung, P., Zheng, Q., Jeffries, D.S., 2018. Estimates of exceedances of critical loads for acidifying deposition in Alberta and Saskatchewan. Atmos. Chem. Phys. 18, 9897–9927.

Malm, W.C., Sisler, J.F., Huffman, D., Eldred, R.A., Cahill, T.A., 1994. Spatial and seasonal trends in particle concentration and optical extinction in the United States. J. Geophys. Res. 99, 1347–1370.

Matsumoto, K., Watanabe, Y., Horiuchi, K., Nakano, T., 2019. Simultaneous measurement of the water-soluble organic nitrogen in the gas phase and aerosols at a forested site in Japan. Atmos. Environ. 200, 312–318.

Meyers, T.P., Finkelstein, P., Clarke, J., Ellestad, T.G., Sims, P.F., 1998. A multilayer model for inferring dry deposition using standard meteorological measurements. J. Geophys. Res. Atmos. 103, 22645–22661.

Murray, W.A., 1981. The 1981 snowpack survey in the AOSERP study area. Prepared for the Alberta Oil Sands Environmental Research Program by Promet Environmental Group, AOSERP Report No. 125:1–137.

NADP, 2019. National Atmospheric Deposition Program (NRSP-3). NADP Program Office, Wisconsin State Laboratory of Hygiene, 465 Henry Mall, Madison, WI 53706. http://nadp.slh.wisc.edu/data/AMoN. Date accessed: September 12, 2019.

Oil Sands Magazine, 2016. Evolution of Mining Equipment in the Oil Sands.

Percy, K.E., 2013. Ambient air quality and linkage to ecosystems in the Athabasca Oil Sands. Alberta. Geosci. Can. 40, 182–201.

Percy, K.E., Hansen, M.C., Dann, T., 2012. Air quality in the Athabasca Oil Sands Region 2011. In: Percy, K.E. (Ed.), Alberta Oil Sands: Energy. Elsevier, Industry and the Environment, pp. 47–92.

Qiu, X., Cheng, I., Yang, F., Horb, E., Zhang, L., Harner, T., 2018. Emissions databases for polycyclic aromatic compounds in the Canadian Athabasca oil sands region – development using current knowledge and evaluation with passive sampling and air dispersion modelling data. Atmos. Chem. Phys. 18, 3457–3467.

Rastogi, N., Zhang, X., Edgerton, E.S., Ingall, E., Weber, R.J., 2011. Filterable water-soluble organic nitrogen in fine particles over the southeastern USA during summer. Atm. Environ. 25, 6040–6047.

Reid, H., Aherne, J., 2016. Staggering reductions in atmospheric nitrogen dioxide across Canada in response to legislated transportation emissions reductions. Atmos. Environ. 146, 252–260.

Sandhu, H.S., Blower, L., 1986. Acid-forming Emissions in Alberta, Canada. Environ. Manag. 10 (5), 689–695.

SEARCH, 2019. SouthEastern Aerosol Research and Characterization network. Atmospheric Research & Analysis, Inc. 410 Midenhall Way, Cary, NC 27513. https://www.dropbox.com/sh/o9hxoa4wlo97zpe/AACbm6LetQowrpUgX4vUxnoDa?dl=0. Date accessed: September 12, 2019.

Seinfeld, J.H., Pandis, S.N., 1998. Atmospheric Chemistry and Physics: From Air Pollution to Climate Change. John Wiley & Sons Inc, New York.

Shotyk, W., Belland, R., Duke, J., Kempter, H., Krachler, M., Noernberg, T., Pelletier, R., Vile, M.A., Wieder, K., Zaccone, C., 2014. Sphagnum mosses from 21 ombrotrophic bogs in the Athabasca Bituminous Sands region show no significant atmospheric contamination of "heavy metals". Environ. Sci. Technol. 48, 12603–12611.

Shotyk, W., Bicalho, B., Cuss, C.W., Duke, M.J., Noernberg, T., Pelletier, R., Steinnes, E., Zaccone, C., 2016. Dust is the dominant source of "heavy metals" to peat moss (Sphagnum fuscum) in the bogs of the Athabasca Bituminous Sands region of northern Alberta. Environ. Int. 92–93, 494–506.

Tang, Y.S., Braban, C.F., Dragosits, U., Simmons, I., Leaver, D., van Dijk, N., Poskitt, J., Thacker, S., Patel, M., Carter, H., Pereira, M., Keenan, P., Lawlor, A., Connolly, C., Vincent, K., Heal, M., Sutton, M., 2018. Acid gases and aerosol measurements in the UK (1999–2015): regional distributions and trends. Atmos. Chem. Phys. 18 (22), 16293–16324.

Tang, H.M., Brassard, B., Brassard, R., Peake, E., 1997. A new passive sampling system for monitoring SO2 in the atmosphere. Field Anal. Chem. Technol. 1, 307–314.

Thompson, T., Rodriguez, M., Barna, M., Gebhart, K., Hand, J., Day, D., Malm, W., Benedict, K., Collett, J., Schichtel, B., 2015. Rocky Mountain National Park reduced nitrogen source apportionment. J. Geophy. Res. Atmos. 120 (9), 4370–4384.

U.S. EPA, 1999. "Compendium of Methods for the Determination of Inorganic Compounds in Ambient Air" Method IO-5.0, June 1999.

UK-AGANET, 2019. © Crown 2019 copyright Defra via uk-air.defra.gov.uk, licenced under the Open Government Licence (OGL). Date accessed: September 12, 2019.

Vijayaraghavan, K., Cho, S., Morris, R., Spink, D., Jung, J.G., Pauls, R., Duffet, K., 2016. Photochemical model evaluation of the ground-level ozone impacts on ambient air quality and vegetation health in the Alberta oil sands region: Using present and future emission scenarios. Atmos. Environ. 141, 209–218.

Wang, X., Chow, J., Kohl, S., Yatavelli, R., Percy, K., Legge, A., Watson, J., 2015. Wind erosion potential for fugitive dust sources in the Athabasca Oil Sands Region. Aeolian Res. 18, 121–134.

Whaley, C.H., Makar, P.A., Shephard, M.W., Zhang, L., Zhang, J., Zheng, Q., Akingunola, A., Wentworth, G.R., Murphy, J.G., Kharol, S.K., Cady-Pereira, K.E., 2018. Contributions of natural and anthropogenic sources to ambient ammonia in the Athabasca Oil Sands and north-western Canada. Atmos. Chem. Phys. 18, 2011–2034.

Xu, W., Luo, X.S., Pan, Y.P., Zhang, L., Tang, A.H., Shen, J.L., Zhang, Y., Li, K.H., Wu, Q. H., Yang, D.W., et al., 2015. Quantifying atmospheric nitrogen deposition through a nationwide monitoring network across China. Atmos. Chem. Phys. 15, 12345–12360.

Zbieranowski, A., Aherne, J., 2012. Spatial and temporal concentration of ambient atmospheric ammonia in southern Ontario, Canada. Atmos. Environ. 62, 441–450.

Zhang, Q., Anastasio, C., Jiminz-Cruz, M., 2002. Water-soluble organic nitrogen in atmospheric fine particles (PM2.5) from northern California. J. Geophys. Res. 107, 4112–4121.

Zhang, J., Moran, M.D., Zheng, Q., Makar, P.A., Baratzadeh, P., Marson, G., Liu, P., Li, S.-M., 2018. Emissions preparation and analysis for multiscale air quality modeling over the Athabasca Oil Sands Region of Alberta, Canada. Atmos. Chem. Phys. 18, 10459–10481.

Zhang, Y., Shotyk, W., Zaccone, C., Noernberg, T., Pellerier, R., Bicalho, B., Froese, D.G., Davies, L., Martin, J.W., 2016. Airborne petcoke dust is a major source of polycyclic aromatic hydrocarbons in the Athabasca Oil Sands Region. Environ. Sci. Technol. 50, 1711–1720.

Zhang, L., Vet, R., O'Brien, J.M., Mihele, C., Liang, Z., Wiebe, A., 2009. Dry deposition of individual nitrogen species at eight Canadian rural sites. J. Geophys. Res. 114, D02301. https://doi.org/10.1029/2008JD010640.